bioRxiv preprint doi: https://doi.org/10.1101/338269; this version posted June 4, 2018. The copyright holder for this preprint (which was not certified by peer review) is the author/funder, who has granted bioRxiv a license to display the preprint in perpetuity. It is made available under aCC-BY 4.0 International license.

Developing A Programmable, Self-Assembling *Squash Leaf Curl China Virus* (SLCCNV) Capsid Proteins Into "Nanocargo"-Like Architecture: A Next-Generation "Nanotool" For Biomedical Applications

Authors and Affiliations

Raja Muthuramalingam Thangavelu¶, Deepan Sundarajan¶, Mohammed Riyaz S.U&, Michael Immanuel Jesse Denison&, Dharanivasan Gunasekaran, Rajendran Ganapathi, Nallusamy Duraisamy, Kathiravan Krishnan*

Plant Molecular Virology and Nanobiotechnology Research Laboratory, Department of Biotechnology, University of Madras, Tamil Nadu, India 600 025.

Author for Correspondence

Kathiravan Krishnan, Assistant Professor, Department of Biotechnology, University of Madras, Guindy Campus, Chennai.

Tel: (+91) 44 22202744

*Author's email ID: drkkathiravan@gmail.com

bioRxiv preprint doi: https://doi.org/10.1101/338269; this version posted June 4, 2018. The copyright holder for this preprint (which was not certified by peer review) is the author/funder, who has granted bioRxiv a license to display the preprint in perpetuity. It is made available under aCC-BY 4.0 International license.

Abstract

A new era has begun in which pathogens have become useful scaffolds for nanotechnology applications. In this research/study, an attempt has been made to generate an empty cargo-like architecture from a high-profile plant pathogen of *Squash leaf curl China virus* (SLCCNV). In this approach, SLCCNV coat protein monomers are obtained efficiently by using a yeast *Pichia pastoris* expression system. Further, dialysis of purified SLCCNV-CP monomers against various pH strengthenened (5–10) disassembly and assembly buffers produced a self-assembled "Nanocargo"-like architecture, which also exhibited an ability to encapsulate the magnetic nanoparticles at *in vitro*. Bioinformatics tools were also utilized to predict the possible self-assembly kinetics and bioconjugation sites as well. The biocompatibility of "SLCNNV-CP-Nanocargo" particles was also evaluated by *in vitro* cancer cells, which eventually proved the particles to be versatile material for the next generation "nanotool" capable of housing various therapeutic or imaging agents.

bioRxiv preprint doi: https://doi.org/10.1101/338269; this version posted June 4, 2018. The copyright holder for this preprint (which was not certified by peer review) is the author/funder, who has granted bioRxiv a license to display the preprint in perpetuity. It is made available under aCC-BY 4.0 International license.

41 # Keywords

42 Plant pathogenic virus; heterologous expression; *in vitro* self-assembly; cargo-like particles;
43 biocompatibility; magnetic nanoparticle encapsulation

44

45

46 # Abbreviations

47 SLCCNV- *Squash leaf curl China virus*, CP- Coat protein, VNPs- Viral nanoparticles, VLPs-
48 Virus-like nanoparticles, HRTEM- High resolution transmission electron microscopy, DLS-
49 Dynamic light scattering, DSC-Differential scanning calorimetry, MTT- [3-(4,5-
50 Dimethylthiazol-2,5-diphenyltetrazolium bromide], IEC- Ion exchange chromatography,
51 MALDI-TOF- Matrix-assisted laser desorption ionization-time of flight, BCAA- Branched-chain
52 amino acid, MNPs-Magnetic nanoparticles

53

54

55

56

57

58

bioRxiv preprint doi: https://doi.org/10.1101/338269; this version posted June 4, 2018. The copyright holder for this preprint (which was not certified by peer review) is the author/funder, who has granted bioRxiv a license to display the preprint in perpetuity. It is made available under aCC-BY 4.0 International license.

Introduction

There has always been a high demand for biological entities which have the ability to act as a multifaceted scaffold or template. Biological entities having intrinsic self-assembling properties are recognized as an excellent aspect in nanotechnology applications [1-4]. The coat protein of viruses are the kind of self-assembling peptides which form a fine architecture at a nanoscale precision is called capsid. Recently viruses are being studied for their ability to self-assemble into the nanoscale particles of discrete size and definite geometry [5-7]. These self-assembling features of viruses have been used as nanoscaffolds for a wide range of innovative applications in various fields such as sensing, imaging, drug delivery, biocatalysis and bioelectronics [8]. Viral nanotechnology is a newly emerging multi-disciplinary area, has begun to manipulate hundreds of both mammalian and plant pathogenic viruses towards the next-generation smart nanodevices [9,10]. The reason of sudden emergence of virus nanotechnology is the search for the solutions to several fundamental challenges in nanoparticles fabrication, that is, controlling the traits of synthetic nanoparticles such as monodispersity, assembly, stability, size and morphology [11]. Viruses derive portions of their structures from peptide-based complexes called 'capsids'. These complexes form nanoscale structures that are often self-assembling, monodispersing, symmetric and stable under general physiological conditions [12, 13]. These tiny structures, also described as viral nano-particles (VNPs) by materials science researchers, possess numerous traits that make them outstanding candidates for nanoresearch. Another superior choice for biomedical researchers is virus-like particles (VLPs), a non-infectious counterpart from plant viruses. These are particularly advantageous because they are less likely to be pathogenic in humans and therefore less likely to induce undesirable side effects [8]. They can be easily produced in sufficient quantities with recombinant technologies. In addition, their

bioRxiv preprint doi: https://doi.org/10.1101/338269; this version posted June 4, 2018. The copyright holder for this preprint (which was not certified by peer review) is the author/funder, who has granted bioRxiv a license to display the preprint in perpetuity. It is made available under aCC-BY 4.0 International license.

properties are easily programmable through changes at the genome level to produce novel functionalities[14].The VLPs that are currently being developed for biomedical applications share the common property of being self-assembling – they form a closed capsid-like structure with an altered symmetryfrom a limited number of protein subunits, which are also referred to by various terms with the prefix of "nano"-cage, -carrier, -cargo, and -container[8]. This states that an interior environment is capable of housing, therapeutic or imaging agents and the exterior environment is capable of multivalent presenting for cell targeting [4,15,16]. There are many studies that have reviewed the self-assembling properties of various kinds of animal and plant virus particles under various *in vitro* conditions such as temperature, pH, and ionic strength [5, 17-22]. In particular, three plant viruses have been studied more than hundred times by various researchers across the country specifically for nanotechnology applications: *Cowpea mosaic virus*, *Cowpea chlorotic mottle virus* and *Tobacco mosaic virus* [8, 23]. Though a few species of viruses have been studied extensively for nanotechnology purposes, there is a need for a new kind of virus that is superior to existing ones. Indeed, exploring novel VNPs or VLPs and their self-assembling properties will lead to novel ideas and concepts for fabrication for human welfare. With this aim, we chose a well-known plant pathogenic virus of the *Begomovirus* isolates of *Squash leaf curl China virus* (SLCCNV) for this study, whose molecular pathogenicity we had already established in our laboratory studies. The true reason for our choice of this virus is no study yet to done to reveal the structural and assembly properties of *Begomoviruses*, which are also crucial for coat-host protein interaction mediated pathogenicity studies.

The *Squash leaf curl China virus* (SLCCNV), a plant pathogenic virus, is one of the 200 species in the *Begomoviruses* genus and belongs to the *Geminiviridae* family [24]. *Begomoviruses* are

bioRxiv preprint doi: https://doi.org/10.1101/338269; this version posted June 4, 2018. The copyright holder for this preprint (which was not certified by peer review) is the author/funder, who has granted bioRxiv a license to display the preprint in perpetuity. It is made available under aCC-BY 4.0 International license.

105 responsible for the huge loss of many economically important crops such as tomatoes, chilly,
106 cassava, squash and cotton [24, 25].The genome of *Squash leaf curl China virus* (SLCCNV) and
107 other members of this genus generally consists of a single-stranded (SS) DNA molecule (5422
108 bp in size). It encodes eight open reading frames, where the AV1 gene (771bp) of the coat
109 protein (CP), represents a twinned icosahedral capsid morphology which encapsulates the whole
110 nucleic acid genome [26]. Interestingly, all members of the *Geminiviridae* have the unique
111 capsid morphology of geminate particles (non-enveloped), consisting of two incomplete T=1
112 icosahedral joined together to produce a structure with 22 pentameric capsomers, made of 110
113 identical CP subunits, each consisting of approximately 30 kDa (256 AA) with an isoelectric
114 point (pI) of 10 [27, 28]. The size of the virus particle is ~38 nm in length and 22 nm in diameter.
115
116 This research work aimed to unveil the self-assembling properties of the native SLCCNV
117 particles as well as *Pichia* expressed SLCCNV coat protein subunits towards. We chose the
118 assembly buffer medium as a reflection of the biological conditions in the intracellular
119 environment [29,30]. To support this experimental study, a detailed *in silico* analysis was also
120 performed to predict the SLCCNV coat protein structure, assembly and its conjugation sites. [31-
121 33]. In vitro A549 cell line studies also demonstrated biocompatible properties of SLCCNV coat
122 protein. A successful *in vitro* self-assembly is valid only if it can be exploited to selectively
123 entrap materials within the mechanisms of the SLCCNV-CP-assembly. By encapsulation with
124 magnetic nanoparticles (MNPs) it was also confirmed [34]. MNPs were used in this study
125 because of their wide range of application ranging from medical diagnosis to treatment [35;36].
126
127

bioRxiv preprint doi: https://doi.org/10.1101/338269; this version posted June 4, 2018. The copyright holder for this preprint (which was not certified by peer review) is the author/funder, who has granted bioRxiv a license to display the preprint in perpetuity. It is made available under aCC-BY 4.0 International license.

Materials and methods

Materials

All the chemicals for growth media and supplements were purchased from Himedia Laboratories, India. Dialysis membrane (15kDa cut-off) also purchased from Himedia Laboratories, India. All the glasswares (Borosil, Scott Duran) and chemicals for buffers and other components for reagents including uranyl acetate and sodium phosphotungstic acid were obtained from Sisco Research Laboratories, India. *E. coli* strains of DH5 alpha, GS115 *Pichia pastoris* strain and pPICZαA plasmid (Invitrogen, USA) for cloning were kind gifts from Prof. S. Meenakshi Sundaram, Centre for Biotechnology, Anna University, Chennai, India. The antibiotic Zeocin was purchased from Invitrogen, USA. For western blotting, the primary polyclonal antibody of DSMZ *African cassava mosaic virus* (ACMV) was used, which was a kind gift from Dr. V. G. Malathi, Distinguished Professor and Virologist, Tamil Nadu Agriculture University, Coimbatore, India. Goat anti-rabbit secondary antibody conjugated HRP enzyme and coat protein-specific forward and reverse primers were obtained from Genei Technologies, Bengaluru. Polyvinylidenedifluoride (PVDF), cloning enzymes and plasmid isolation kits were purchased from Thermo Fischer and Fermentas, Hyderabad. The TAS-ELISA kit for ACMV was purchased from DSMZ, Germany. For chromatography, pre-packed HiTrap ion exchange columns were purchased from GE Healthcare, India. For cell line studies, A549 lung cancer lines were obtained from the NCCS cell repository, Pune. Acetaminophen, potassium bromide and MTT [3-(4,5-dimethylthiazol-2,5-diphenyltetrazolium bromide] were obtained from Sigma-Aldrich, India. Ham's F12-K medium and TPVG were purchased from Himedia, India. Foetal bovine serum (FBS) and Antibiotic-Antimycotic was from Gibco Life

bioRxiv preprint doi: https://doi.org/10.1101/338269; this version posted June 4, 2018. The copyright holder for this preprint (which was not certified by peer review) is the author/funder, who has granted bioRxiv a license to display the preprint in perpetuity. It is made available under aCC-BY 4.0 International license.

Technologies, USA. Ferrous chloride hydrated extra pure (code no. 03846) and ferric chloride anhydrous 98% extra pure (code no. 03817) were obtained from LobaChemie Pvt. Ltd, India.

Isolation and purification of virus particles

To investigate the assembling and disassembling processes, native *Squash leaf curl China virus* (SLCCNV) was isolated from the natural host *Benincasa hispida* (winter melon), which was collected from a field at Perambalur in the southern part of the state of Tamil Nadu in India. Further, screenings and confirmations were made by molecular studies including PCR amplification with coat protein-specific primers, which was already reported in our previous work [37]. The virus particles or so-called viral nanoparticles (VNPs) were purified by cesiumsulfate (Cs_2SO_4) density gradient ultracentrifugation (CP100WX, HITACHI, JAPAN) using fixed angle rotor P100AT2 (803,000xg) and swing bucket rotor P55ST2 (366,000 x g) with necessary modifications [38]. Purified fractions of virus proteins were collected and dialyzed against 0.1M phosphate buffer (pH 7.2) to remove the remnants of Cs_2SO_4. The purity of the native virus particles was also confirmed through SDS-PAGE followed by a western blot analysis [39,40]. For experimental control, the purified native virus particles were used all along with SLCCNV-CP subunits to be expressed in yeast *Pichia pastoris*.

Heterologous expression of SLCCNV-CP in yeast *Pichia pastoris*

The coat protein expression comprises three principal steps: (a) insertion of the gene into an expression vector; (b) transformation of the expression vector into the *P. pastoris*host; (c) examination of potential strains for the expression of the SLCCNV-CP gene. The methylotrophic yeast *Pichia pastoris* GS115 strain was applied as a host cell to express SLCCNV coat protein [41]. The plasmid pPICZαA containing methanol-inducible AOX1 promoter was used to

bioRxiv preprint doi: https://doi.org/10.1101/338269; this version posted June 4, 2018. The copyright holder for this preprint (which was not certified by peer review) is the author/funder, who has granted bioRxiv a license to display the preprint in perpetuity. It is made available under aCC-BY 4.0 International license.

172 construct the full length SLCCNV coat protein gene [42]. The major advantage of using
173 pPICZαA (3.6 kb) vector for expression is the presence of a Zeocin-resistant gene for selection,
174 which has an alpha-factor secretion signal for directing the secreted expression of the
175 recombinant protein into the growth medium [43].

176 **Construction of expression vector**

177 To design an insert for expression, a complete coat protein gene (771bp) from the AV1 region of
178 DNA-A of SLCCNV was taken from our own nucleotide deposit in the NCBI repository
179 (GenBank accession no.**KF188433.1**) [37]. The sense and anti-sense primers KKCPF-5'-
180 CCGGAATTCATGGCGAAGCGACCACCACCAGATA-3' and KKCPR-5'-CCGGGTACCAT
181 TTGTTACCGAATCCATAAAA-3' capable of generating a 771-bp coat protein gene fragment
182 (256 amino acids) containing double restriction enzyme sites (*Eco*RI and *Kpn*I) were designed
183 using the BioEdit 7.1 software [44]. To express the pure form of SLCCNV coat protein without
184 the C-terminal peptide, stop codon (5' cap, *poly*-A tail) had been included in the anti-sense
185 primer. By PCR amplification, the double-stranded oligonucleotide fragments corresponding to a
186 CP protein of SLCCNV, with *Eco*RI and *Kpn*I cohesive ends, were obtained by annealing (63˚C
187 -65˚C) the sense and anti-sense primers using the whole SLCCNV genome as a template. The
188 PCR-obtained CP gene fragments of SLCCNV were inserted into multiple cloning sites (MCS)
189 of pPICZαA vector in the C-terminal in-frame fusion. In brief, the inserts of the CP gene and
190 pPICZαA vectors were appropriately digested with restriction enzymes *Eco*RI and *Kpn*I. An
191 enzyme-excised fragment was inserted between the *Eco*RI and *Kpn*I sites of the pPICZαA
192 vector, yielding clone plasmids of pPICZαA-SLCCNV-CP. The final construct was confirmed
193 by restriction mapping with the same digestive enzymes. Following this, a propagation of vector
194 was performed by the transformation of those clones into *E. coli* DH5-α-competent cells derived

bioRxiv preprint doi: https://doi.org/10.1101/338269; this version posted June 4, 2018. The copyright holder for this preprint (which was not certified by peer review) is the author/funder, who has granted bioRxiv a license to display the preprint in perpetuity. It is made available under aCC-BY 4.0 International license.

from calcium chloride, which was screened and then cultured in a low-salt LB medium containing the Zeocin antibiotic (25µg/ml). Furthermore, all expression steps were performed according to the manual given by Easyselect™ *Pichia* expression kit (Invitrogen) with necessary modifications.

Transformation, screening and confirmation of Mut$^+$ phenotype

For *P. pastoris* transformation, the host cells were washed in two simultaneous steps with Milli-Q water and 1M sorbitol, based on manufacturer guidelines. The 100µl of the fresh, competent GS115 *P. pastoris* cells plus 10µg of linearized (*Sac*I enzyme digested) plasmid DNA was pulsed in 0.1 cm electroporation cuvettes (Model.No.620, BTX, Harvard apparatus, Holliston, USA) at 1.5 kV, 50 F, 250 Ω and 10–12 millisecond (Bio-Rad gene-pulser).The transformed cells were selected on YPD (Yeast extract peptone dextrose) Zeocin plates and then screened for the insert by PCR on isolated yeast genomic DNA using 5' and 3'AOX1 (5'-GACTGGT TCCAATTGA CAAGC-3'and 5'-GTCCCTATTTCAATCAATTGAA-3'). Screening of recombinants was confirm with SLCCNV coat protein, specific primers at 771bp. Subsequently, positive clones were used for the analysis of the methanol-utilizing phenotype. The Mut+ phenotype for the transformed GS115 cells was determined by growing clones on a minimal methanol medium with histidine (MMH) and a minimal dextrose medium with histidine (MDH) plates. A single transformed colony of GS115 was grown in 200ml of BMGY (Buffered Glycerol-Complex Medium) at 28–30˚C and at the agitation rate of 250 RPM. The cells (OD600 = 2-6) were harvested and resuspended in 500 ml of BMMY (Buffered Methanol-Complex medium) in a 1L triple-side baffled flask (OD600 = 1.0) to induce expression at 28–30˚C. Absolute methanol was added to a final concentration of 0.5% every 24 hours to maintain induction for up to four days. Each day, 1ml of the supernatant was collected to optimize the

bioRxiv preprint doi: https://doi.org/10.1101/338269; this version posted June 4, 2018. The copyright holder for this preprint (which was not certified by peer review) is the author/funder, who has granted bioRxiv a license to display the preprint in perpetuity. It is made available under aCC-BY 4.0 International license.

protein expression profile of transforming Mut^+ phenotype cells. The collected supernatant was subjected to electrophoretic separation on a 12% polyacrylamide gel (SDS-PAGE) and stained by silver nitrate according to the standard procedure [39]. Following electrophoresis, proteins were electrotransferred onto a PVDF membrane and immunoblotted with an ACMV primary antibody specific to the *Begomovirus* coat protein. The secondary HRP enzyme conjugated antibody used to detect the protein of interest at the end [40]. The concentrated supernatant of GS115 transformed with an empty vector (pPICZαA) was used as the negative control in both tests. The percentage of *Pichia*-expressed SLCCNV-CP was then determined by ELISA with the known concentration of the ultracentrifuge-purified native virus protein as a positive control [40].

Purification and characterization of expressed SLCCNV-CP

At the end of the fourth day of culture in BMMY, the supernatant was harvested by high-speed cooling centrifugation (10000 RPM), after it was concentrated (10- to 100-fold) by the usage of 75% ammonium sulphate precipitation [46]. The precipitant was further dialyzed against a 0.1M phosphate buffer (pH 7.2) to eliminate the ammonium salts. Then the concentration of protein was determined by absorbance measurement at 280nm (1cm path length) with an extinction coefficient of 3.4. The ion exchange chromatography (IEC) purification was performed based on the chromato-focussing method. This method was chosen to separate the SLCCNV-CP according to the pI (isoelectric point) and its theoretically determined pKa values [17]. To purify the coat protein from the active ammonium sulfate fraction, one millilitre of the fraction was loaded into the ACTA purifier (GE Healthcare) in 5ml of HiTrap ion exchange column. The column was pre-equilibrated with buffer A and buffer B. The unbound proteins were washed with the same buffer and the bound proteins were eluted by a linear gradient of salt (1M NaCl) with a flow rate

bioRxiv preprint doi: https://doi.org/10.1101/338269; this version posted June 4, 2018. The copyright holder for this preprint (which was not certified by peer review) is the author/funder, who has granted bioRxiv a license to display the preprint in perpetuity. It is made available under aCC-BY 4.0 International license.

of 1 ml/min. The eluted fractions containing the SLCCNV-CP were pooled and stored at -80˚C. The obtained fractions were analyzed at 12% SDS-PAGE. Following electrophoresis, SDS-PAGE bands containing the protein of interest were excised from stained gels and subjected to the in-gel trypsin digestion procedure as described elsewhere [47, 48]. Spectral measurements were taken using an Ultraflex III MALDI-TOF/TOF instrument (Bruker Daltonics, Germany)in the positive ion reflector mode for acquiring the peptide mass fingerprint (PMF) at the International Center for Genetic Engineering and Biotechnology (ICGEB), New Delhi, India. Tandem mass spectrometry-based fragmentation was employed to identify the protein from the observed peptide precursor ions. The instrument parameters for PMF (peptide mass fingerprinting) and MS/MS analysis were set as described elsewhere [48]. The fragmented peptides were analyzed using flexAnalysis software (version 3.0) and sent to database search using BioTools software (version 3.2). The database search parameters were set as described [48] and fragment masses with MS tolerance of up to +/-100 ppm and MS/MS tolerance of up to +/-0.75 Da were searched in the NCBInr database. The following criteria were used for identification: (i) significance threshold was set to achieve $p<0.05$, (ii) the expectancy cut-off was set to 0.05, and (iii) individual ion score ≥ 45 was only considered for identification.

Investigation of self-assembly of SLCCNV (native and *Pichia*-expressed)

In vitro assembly were performed by the conventional dialysis method (15kDa cut-off membrane) against various pH assembly buffers. The assembly buffers with different pH (5 – 10) were prepared by the addition of 1mM $CaCl_2$ [29,30,49, 50]. In the first study, small volume of native SLCCNV particles presence in the buffer of pH 7.2 (0.1M phosphate buffer) were dialysis against the buffer of pH 5.0 (0.1M sodium acetate) at the cold temperature for 8 hours.

bioRxiv preprint doi: https://doi.org/10.1101/338269; this version posted June 4, 2018. The copyright holder for this preprint (which was not certified by peer review) is the author/funder, who has granted bioRxiv a license to display the preprint in perpetuity. It is made available under aCC-BY 4.0 International license.

After that, the existing buffers in dialysis tank were exchanged to the other assembly pH buffers of pH of 6.0 - 8.0 (0.1M sodium phosphate), pH 9.0 (0.1M sodium borate) and pH 10.0 (0.1M sodium glycine) at the stipulated time period of 8 hours in cold conditions. Eventually, the same dialysis procedure were carried out for *Pichia*-expressed SLCCNV-CP subunits. Meanwhile small aliquots of the dialyzed samples from the different assembly pH buffers were taken to the study by High-resolution transmission electron microscopy (HRTEM-FEI, TechnaiG2, 30S-TWIN D905, USA) and dynamic light scattering (DLS, Malvern Instruments Ltd., Malvern, UK). For the HRTEM analysis, the specimens were processed with a 2% negative stain of sodium phosphotungstate and uranyl acetate prepared at neutral pH. From the HRTEM micrograph, it was observed that the sodium phosphotungstate-stained samples were clearer than the uranyl acetate-stained samples [51].

In silico analysis of SLCCNV coat protein

Initially, a converted FASTA format of a coat protein-related amino acid sequence (accession no. **KF188433.1**)[37] was submitted to the I-TASSER (Iterative Threading Assembly Refinement) server [31,52]. Kind of similar protein structure templates were threaded through the PDB library by LOMETS, a locally installed meta-threading approach. The excised PDB templates were reassembled into full-length models using Monte Carlo simulations, with the threading unaligned regions built by *ab initio* modelling. When no appropriate templates were identified by LOMETS, the whole protein structures were built by *ab initio* modelling. SPICKER identified low free energy state through clustering of the simulation decoys. Finally, TMalign was used to align the LOMETS templates and the PDB structures. The final full atomic models were obtained from the I-TASSER decoys by REMO [45]. Further, it was validated through UCLA-

bioRxiv preprint doi: https://doi.org/10.1101/338269; this version posted June 4, 2018. The copyright holder for this preprint (which was not certified by peer review) is the author/funder, who has granted bioRxiv a license to display the preprint in perpetuity. It is made available under aCC-BY 4.0 International license.

DOE (http://nihserver.mbi.ucla.edu/Verify-3D/) structure evaluation server, which gives a visual analysis of the quality of a putative crystal structure for proteins. The structural models were validated using PROCHECK [45]. The query-modelled protein structure was submitted as PDB files on the SAVES server (http://nihserver.mbi.ucla.edu/SAVES/) [53,54]. The quality of the protein structure was validated from the Ramachandran plot through the Procheck server [55].

Prediction of assembly of SLCCNV-CP monomers

The PatchDock server is a simple and intuitive web interface, available at http://bioinfo3d.cs.tau.ac.il/PatchDock [56]. The I-TASSER-derived monomeric structure of SLCCNV coat protein was uploaded to the server and a docking request was submitted. Once the prediction process was completed, the results were received by email containing the web link for the predicted page. Modelling was performed to assemble a pentameric coat protein structure and the it was repeated at three times. At the end of the process, pentameric structure of the SLCCNV capsid protein was received. In addition, we tried to predict the solvent accessible surface areas (SASA) by Accelrys Discovery Studio 2.5, because it was believed that one of the key factors involved in the coat protein subunit assembly. Therefore, each modelled protein structure (monomer to pentameric) was uploaded in Accelrys Discovery Studio 2.5 [57]. The Connelly-type solvent accessibility helped in the identification of buried and exposed residues in the solvent system. The solvent-exposed and buried residues were displayed as red and blue colour, respectively.

Analysis of binding sites and surface functional groups in the SLCCNV-CP

Molsoft ICMPro is a very useful bioinformatics tool in the analysis of protein structure. The tools included in the ICM Pro are calculating RMSD, identifying closed cavities, calculating

bioRxiv preprint doi: https://doi.org/10.1101/338269; this version posted June 4, 2018. The copyright holder for this preprint (which was not certified by peer review) is the author/funder, who has granted bioRxiv a license to display the preprint in perpetuity. It is made available under aCC-BY 4.0 International license.

309 contact and surface area, measuring angles, distances and generating Ramachandran plots [58].
310 The pentameric protein structure was loaded into the Molsoft ICM-Pro molecular software for
311 the analysis of binding sites and surface groups. The protein structure was loaded into the
312 software window and converted into an ICM object for further process. The ICM-converted
313 protein structure was used for the prediction of binding sites and the residues on the surface of
314 the protein. With the same bioinformatics tool, the possible bioconjugation sites were also
315 identified in the ICM object. The predicted bioconjugation sites were indicated as molecular
316 surfaces in the 3D ribbon diagram of SLCCNV coat protein.
317

318 **Biocompatibility test**

319 General biocompatibility or toxicity tests, aimed mainly at detection of the biological activity of
320 test substances, can be carried out in many cell types (e.g. fibroblasts, HeLa, hepatoma cells)
321 [59]. In this research/study, the biocompatibility feature of the expressed SLCCNV-CP alone
322 was determined in a dose-dependent manner by the MTT assay with A549 lung cancer cell line.
323 [60]. The A549 cells (1×104) were seeded onto 96 well flat-bottom culture plates and incubated
324 for 24 hours at 37˚C with 5% of CO_2 to reach the confluence in 70%. Over thirty various
325 concentrations of SLCCNV-CP (0.54 to18 µg/ml) were tested against the cell culture seeded in
326 the 96 well plate. The treated cells were kept incubated for 24 hours, after which 10µL of MTT
327 (5mg/ml in PBS) added to each well and the plate was incubated for another four hours at 37ºC.
328 The resulted formazan crystal was dissolved in 100µL of DMSO (Dimethyl sulfoxide) with a
329 gentle shake and the absorbance was measured at 595nm using an ELISA reader (BioTek power
330 wave XS, USA). All these steps were replicated at three times independently and the average has

bioRxiv preprint doi: https://doi.org/10.1101/338269; this version posted June 4, 2018. The copyright holder for this preprint (which was not certified by peer review) is the author/funder, who has granted bioRxiv a license to display the preprint in perpetuity. It is made available under aCC-BY 4.0 International license.

been shown as a cell viability percentage in comparison with the control experiments, where the SLCCNV-CP untreated controls were considered as 100% viable.

Cytotoxicity%=[1-($OD_{treated}$/$OD_{control}$)]*100

where $OD_{treated}$ and $OD_{control}$ corresponded to the optical densities of treated and control cells. The percentage of cytotoxicity (%) plotted as a function of concentration, fitted to a sigmoidal curve and the median inhibitory dose (IC_{50}) value was determined on the basis of this curve. The IC_{50} represents the concentration of *Pichia*-expressed SLCCNV-CP required to achieve 50% inhibition of cell growth at *in vitro*.

Encapsulation efficiency of SLCCNV-CP-Nanocargo on magnetic nanoparticles

To evaluate the encapsulation efficiency of SLCCNV-CP-Nanocargo, negatively charged magnetic nanoparticles (MNPs) with the mean size of ~25nm were used. The magnetic nanoparticles (MNPs) were prepared using the co-precipitation method followed by a slight modification of protocol, which has been reported by us earlier [61]. To assemble the SLCCNV-CP over MNP core, one equivalent of MNPs (about 5.2µg/ml) was mixed with 100 equivalents of SLCCNV-CP monomers and first dialyzed against a pH 6 disassembly buffer at 4˚C for overnight (~12 hours). Subsequently, the samples were collected and freshly dialyzed against an assembly buffer of pH 7 at 4˚C in order to re-assemble the SLCCNV-Nanocargo with MNPs. Finally, the dialyzed samples were pooled and centrifuge at 50,000g for 1hour at 4˚C and then the pellet containing the samples was resuspended in 100µl of a 0.1M phosphate buffer (pH 7.2). The samples were stored at -20˚C until use. The encapsulation efficiency of SLCCNV-CP was determined by UV-Vis spectroscopy, HRTEM coupled with energy dispersive X-ray

bioRxiv preprint doi: https://doi.org/10.1101/338269; this version posted June 4, 2018. The copyright holder for this preprint (which was not certified by peer review) is the author/funder, who has granted bioRxiv a license to display the preprint in perpetuity. It is made available under aCC-BY 4.0 International license.

spectroscopy (HRTEM-FEI, TechnaiG2, 30S-TWIN D905, USA) and 8% native polyacrylamide gel electrophoresis.

Results

SLCCNV-CP expressed by yeast *Pichia pastoris*

The expression of the entire *Begomovirus* unmodified coat protein subunits was first achieved in the eukaryotic yeast *Pichia pastoris* system. The PCR-amplified product corresponding to the full-length coat protein gene of 771bp is shown in the agarose gel image (Figure 1A). The double-enzyme (*Kpn*I & *Eco*RI) digested restriction map of the expression cassette of pPICZαA-SLCCNV-CP was reviewed which provides the product length of 3.6 kb for the pPICZαA vector and 771bp for the CP gene, whereas undigested gives 4.4 kb (Figure 1B). The cloned expression vectors were successfully propagated into recA1- and endA1-deficient *E. coli* DH5-α strains with good yield. The DNA sequencing results of AOX1 5' and 3' primer-amplified PCR products determined that our recombinant construct had an insert in the correct orientation (sequencing data not included). An enzyme (*Sac*I)-linearized vector of pPICZαA-SLCCNV-CP (4.4kb) was successfully electrotransferred to GS115 cells, which yielded Zeocin-resistant *Pichia* recombinants that were screened and confirmed by culturing them with Zeocin antibiotics (Figure 1C&D)**.** In figure 1E,the gel image shows PCR-amplified products at 771bp and 500bp with CP gene-specific primers confirming the presence of the CP gene in the genome of *Pichia* recombinant colonies. The recombinants cultured in BMMY growth medium yielded the SLCCNV-CP protein by secretion, which was collected by centrifugation and confirmed in the protein denaturing gel. In figure 1F, silver stained gel image of SDS-PAGE, lane 1 shown the multiple protein bands for the supernatant collected from the transformed colonies and the lane 2

bioRxiv preprint doi: https://doi.org/10.1101/338269; this version posted June 4, 2018. The copyright holder for this preprint (which was not certified by peer review) is the author/funder, who has granted bioRxiv a license to display the preprint in perpetuity. It is made available under aCC-BY 4.0 International license.

dedicated to the non-transformed colonies shown only few bands. An another SDS-PAGE performed with both purified native SLCCNV particles (Figure 1G lane1) and *Pichia* expressed CP monomers (Figure 1G lane 2) has shown some equivalency at the high molecular weight bands. The purified expressed SLCCNV-CP monomers in the gel, shown multiple bands of different molecular weight and one at 30kDa corresponding to the MW of SLCCNV-CP monomer (Figure 1G lane 2). In the denaturing gel with native virus particles (Figure 1G lane1), presence of high MW bands might represent the stable capsomeric architecture (Virus/110monomers/30kDa=3,300kDa). We surprised of the stability of the native virus particles against common protein denaturing conditions. Even at a twofold increased concentration of reducing agents (β-mercaptoethanol and Dithiothreitol) and SDS, the native virus particles remains intact and not yield any monomeric protein bands in the gel. Finally, the intact native virus particles denatured at 10 min incubation in high temperature (85˚–90˚C). It has given two denatured bands with a high molecular weight close to one another. Meanwhile, to confirm the native virus stability in the temperature, a Differential Scanning Calorimetry (DSC) was performed [62]. The DSC result indicated that the whole virus particles were intact and stable up to 75˚C. It was only started to denature at the temperature above 80˚C (Figure S1, supplementary information), thus added one more evidence of the stability of virus particles.

This phenomenon was also confirmed after performing the confirmative assay of western blot using an ACMV polyclonal antibody and an HRP-conjugated secondary antibody with DAB (3, 3'-diaminobenzidine) substrate. In the Figure 1H, the blotting membrane showed the bands corresponding to the protein samples similar in the previous SDS-PAGE gel picture (Figure 1G). A single intensified band that is exactly the same size observed in the SDS-PAGE for native

bioRxiv preprint doi: https://doi.org/10.1101/338269; this version posted June 4, 2018. The copyright holder for this preprint (which was not certified by peer review) is the author/funder, who has granted bioRxiv a license to display the preprint in perpetuity. It is made available under aCC-BY 4.0 International license.

virus particles observed in the Figure 1H Panel 1. Another western blot (Figure 1HPanel 2) with *Pichia*-expressed SLCCNV-CP showed two high-intensity bands roughly equivalent to coat protein monomers in 30kDa, and multimers of capsomers which were similarly observed in SDS-PAGE. The high yield of SLCCNV coat protein monomers was achieved by inducing the culture of *Pichia* recombinants with 0.5% methanol at different time points (4 days), which yielded a threefold increase in the overall concentration of protein on the last day (compared to the first day), as quantified by ELISA (Fig.S2., supplementary data). The untransformed cultures of *Pichia* cells (control) in the BMMY medium decreased in growth (OD_{600} at 3 to 1) in the presence of methanol from the second day itself. It shows that untransformed colonies are much more susceptible to methanol due to the absence of a methanol-utilizing gene/vector.

Ion exchange chromatography and MALDI-TOF

The active fraction from the ammonium sulphate fractionation was loaded into a weak cationic ion exchange chromatography [CM-Sepharose Fast Flow 5ml column]. Initially, the column was pre-equilibrated with buffer A (20 mM Tris, pH 6.0, containing 150mM NaCl). The protein was unabsorbed by the column [Fig.S3.,Supplementary information(inset CM-ion exchange profile image)]. After this, the unbound protein from the CM -Sepharose was adjusted to pH 7.8 and loaded onto a strong anionic Qff 5ml column. Unbound proteins were collected as flow-through with Buffer A, [20mM pH 7.8 containing 150mM NaCl about 6 CV (column volume)] and the bound proteins were eluted at about 12 CV by Buffer B (20mM Tris pH 7.8 +1M NaCl) using a linear gradient method. Figure S3., (Qff-ion exchange profile image) shows the elution profile of the active fraction. It is clear that flow-through proteins do not contain the protein whereas the elution fractions show the purified protein. Homogeneity and purity of the elution fraction was

bioRxiv preprint doi: https://doi.org/10.1101/338269; this version posted June 4, 2018. The copyright holder for this preprint (which was not certified by peer review) is the author/funder, who has granted bioRxiv a license to display the preprint in perpetuity. It is made available under aCC-BY 4.0 International license.

423 determined through 12% SDS-PAGE (fig.S3. insetSDS-PAGE image). In SDS-PAGE, a similar
424 banding pattern of multiple protein bands was observed at a different molecular weight that
425 represents the monomeric (30kDa) and multimeric forms of coat protein. These multimers can
426 either be dimer, trimer, tetramer, pentamer or hexamer. In addition, high MW protein bands were
427 excised and utilized for the MALDI analysis. The ELISA quantified the final concentration of
428 the purified *Pichia*-expressed SLCCNV coat protein monomers was 0.57mg/ml which also
429 twofold higher than the ultracentrifuge purified native virus protein (0.241mg/ml) (Figure S2).
430 The protein sequence information obtained from MALDI-TOF/TOF of a single excised coat
431 protein spot was submitted to the MASCOT search engine (Matrix Science Ltd.). The MASCOT
432 results showing the list of all entries from the NCBInr for known protein sequences matched the
433 experimental peptide sequence data (Figure 2). It revealed that PMF (protein mass fingerprint)
434 obtained from MALDI-TOF/TOF analysis from the 1D gel was identical to the *Squash leaf curl*
435 *China virus* and the protein coverage was achieved at 39%. Twelve peptides were matched with
436 the *Begomovirus* coat protein sequence profile through an analysis using the NCBI database. The
437 protein scores achieved greater than 74. The predicted molecular mass (30kDa) and pI (10) value
438 of the expressed SLCCNV-CP were found to be identical with the *Begomovirus* isolates and
439 particularly the *Squash leaf curl China virus* of the Thailand strain.

440 **Self-assembly of SLCCNV (native and *Pichia*-expressed CP monomers)**

441 Early investigation of disassembly and assembly of native SLCCNV particles through electron
442 microscopy, we found that there was no evidence of either particle disassembly or assembly
443 observed in the virus samples dialyzed against various pH buffers (5 to10). In figure 3A-C Panel
444 2, the HRTEM micrographs clearly show that the native virus particles remained intact, with
445 slight morphological transitions, when dialyzed against the pH 7-9 buffers. At pH below the 7, a

bioRxiv preprint doi: https://doi.org/10.1101/338269; this version posted June 4, 2018. The copyright holder for this preprint (which was not certified by peer review) is the author/funder, who has granted bioRxiv a license to display the preprint in perpetuity. It is made available under aCC-BY 4.0 International license.

446 slightly denatured structure and aggregated particles were observed, which was definitely not the
447 disassembly of particles. Because the virus particles sizes remained same at the measurement of
448 HRTEM bar scale. At pH 10, the native virus particles were found in aggregated state (Figure 3C
449 Panel 2 HRTEM image). The data obtained from DLS also supported the evidence of electron
450 microscopic observation which was determined that the native SLCCNV particles were intact by
451 their size (mean ~36nm) on the pH of 7 to 9, and they aggregate at the pH >7 and pH <9 which
452 resulted in the increased mean hydrodynamic size of the particles. The obtained DLS data is/has
453 been exhibited as a graph (Figure 3A-C Panel 1) and the calculated mean hydrodynamic
454 diameter (D_H) is plotted against the corresponding dialyzed pH buffers and then represented in a
455 graph (Fig.S4.B, supplementary data).With the direction of obtained knowledge from self-
456 assembly study of the native virus particles, a closer investigation of the self-assembling kinetics
457 of *Pichia*-expressed SLCCNV-CP was performed using the same DLS and electron microscopy
458 instruments. Here, all the HRTEM and DLS data is represented by graphs and figures (Figure 4
459 & 5). The electron micrographs obtained from HRTEM has clearly described the valid structural
460 transition of SLCCNV-CP in the respective assembly pH buffer. However, we have never seen
461 such remarkable stages of spontaneous *in vitro* virus coat protein assembly in any previous
462 studies [74].The *Pichia*-expressed CP dialyzed against the buffer pH 5 in the negatively stained
463 HRTEM micrographs show that the CP monomers are in a completely disassembled state,
464 possibly being in an unfolding condition due to acidic buffer medium, which was also
465 determined by DLS hydrodynamic size measurement (Figure 4APanel 1-3). It was determined
466 that there particles of an average size of ~30 nm were present in the pH 5 buffer medium. We
467 also obtained a negative measurement value, which meant that size undetermined particles were
468 present in the buffer medium. When we observed an event of self assembly of the SLCCNV-CP

bioRxiv preprint doi: https://doi.org/10.1101/338269; this version posted June 4, 2018. The copyright holder for this preprint (which was not certified by peer review) is the author/funder, who has granted bioRxiv a license to display the preprint in perpetuity. It is made available under aCC-BY 4.0 International license.

469 at buffer pH 6, the results in the HRTEM micrograph were surprising. In figure 4B Panel 2, the
470 electron micrograph shows a spectacular array made of coat protein monomers that can be a
471 disassembling event as was clearly visualised in the electron micrograph in the 100nm bar scale.
472 It has an average size of ~300nm which was also confirmed by DLS(Figure 4B Panel 1). We
473 confirm a speculation about the particular disassembling event of CP monomers at the pH of 6
474 after analyzing the results of buffer pH 7 further. However, at pH 7, a nanoscale structure that
475 collectively organized and assembled by CP monomers into a cargo-like architecture was
476 observed (Figure 4C Panel 2). In the same micrograph, a single twin icosahedral structure similar
477 to the structure of *Begomovirus* (geminate) was also observed. The DLS data also confirmed that
478 the self-assembled arrayed particles were present in a single population within the mean
479 hydrodynamic size of ~250nm (Figure 4C Panel 1). Significantly, SLCCNV-CP particles
480 dialyzed at a assembly buffer pH of 8 on the electron micrograph buffer were detected as as
481 intact, well dispersed and having multiple spherical-shaped (cargo-like) architectures with one
482 geminate like structure on the electron micrograph (Figure 5A Panel 2). The DLS results also
483 greatly correlated with the HRTEM observation and it was shown that the structures were in a
484 highly dispersed state, with two different sizes of population ranging at ~60nm and ~510nm
485 (Figure 5A Panel 1). In the SLCCNV-CP dialyzed at a assembly buffer pH 9, there was no
486 evidence of cargo-like structures observed in this HRTEM micrograph (Figure 5B Panel 2).
487 Also, we observed aggregated population of CP monomers in the same electron micrograph. The
488 DLS for the same (pH 9) buffer medium also revealed that there were two populations of
489 aggregated particles with the size of ~100nm and ~700nm (Figure 5B Panel 1). The CP
490 monomers in the buffer pH at 10, small-to-large population of protein aggregates were observed
491 in the size ranges at ~50nm and ~1100nm (figure 5C Panel 2). Also, the DLS data were

bioRxiv preprint doi: https://doi.org/10.1101/338269; this version posted June 4, 2018. The copyright holder for this preprint (which was not certified by peer review) is the author/funder, who has granted bioRxiv a license to display the preprint in perpetuity. It is made available under aCC-BY 4.0 International license.

492 confirmed the same, whereas 90% of protein particles were in the aggregated state at the buffer
493 pH 10 (Figure 5C Panel 1). Overall, it was determined that the rate of self-assembly of
494 SLCCNV-CP was greater at the pH of 8. Finally, through DLS calculated mean hydrodynamic
495 diameters (D_H) for SLCCNV-CP in the presence of different pH were plotted against the
496 corresponding dialyzed pH buffers (Fig.S4.B, supplementary data).

497 The data for the self-assembly of SLCCNV-CP at varying pH with calcium ions point out that
498 many of the observed effects were a result of the charging of the SLCCNV-CP and their
499 interaction with the pH medium. To interpret the results, we evaluated the capsid net charge on
500 the basis of its peptide sequence against its respective pKa values at varying pH using an online
501 bioinformatics tool [63]. In Fig.S4.A, supplementary data, data summation shows that the pH at
502 which this net charge equals zero could be the theoretical isoelectric point (pI) for both SLCCNV
503 native and expressed coat protein. Below the pI, the SLCCNV-CP has a net positive charge due
504 to the protonation of hydrogen ions to the amino acids. The bioinformatics tool provides a logical
505 estimation of the SLCCNV coat protein net charge in the respective buffer.

506 ## *In silico* analysis of SLCCNV coat protein

507 ### Modelling of monomeric protein structure in I-TASSER

508 The protein structure was modelled using I-TASSER, a hierarchical approach to predict the
509 structure and function of an unknown protein from its sequence. The server generated the ten
510 best models of protein structure, from which the best one was selected based on the C-score
511 [64].The C-score of the predicted protein model was -2.45. The C-score of another predicted
512 model was significantly higher and hence model 1 was chosen for further study (Figure 6A). The
513 overall quality of the predicted protein models was evaluated using the RMSD and the TM-

bioRxiv preprint doi: https://doi.org/10.1101/338269; this version posted June 4, 2018. The copyright holder for this preprint (which was not certified by peer review) is the author/funder, who has granted bioRxiv a license to display the preprint in perpetuity. It is made available under aCC-BY 4.0 International license.

514 score, which are 0.8±0.2 and 14.2±2, respectively. The I-TASSER method was used for the
515 prediction of protein structures with very little or no similarity, since the monomeric protein
516 structure was not available in any of the protein data repositories [45]. The predicted protein
517 model was validated on the SAVES PROCHECK server. The server constructed a
518 Ramachandran plot expressing the quality of the predicted protein model (Figure 6B). The result
519 shows that 67% of the residues are found in the favoured region, while 24% of residues are in
520 allowed region and 9.1% of residues are in the outlier region. The 21 residues of Pro13, Arg19,
521 Phe23, Tyr27, Thr45, Arg51, Cys68, Arg80, Asp82, Ser113, Lys119, Asp123, Glu124, Asn125,
522 Lys127, His131, Phe159, Ser193, Phe202, Tyr219 and Asn238 were found in the outlier region.
523 The reduced quality of the predicted protein structure was due to the amino acid residues in the
524 outlier region. The less availability of similar protein templates resulted in the low quality of plot
525 [55].

526 **Assembly of monomeric subunits into multimers**

527 The SLCCNV-CP subunits were docked to assemble the monomeric units into a pentameric
528 form of a viral capsid symmetry using a PatchDock online server. The docking method was
529 performed with an RMSD of 4.0. The docking of monomer–monomer, dimer–monomer, trimer–
530 monomer and tetramer–monomer was carried out in four cycles to get a pentameric structure
531 (Figure 6A).The structure was obtained with five subunits of monomer possessing secondary
532 structures for each subunit. The atomic contact energy (ACE) score was observed for each
533 subunit assembly (Table 1). The docking area increased with an increase in the number of
534 subunits, which has relatively decreased the contact energy resulting in the efficient binding of
535 two protein structures. The atomic contact energy score is based on the number of water contacts
536 replaced by the atomic contacts from the proteins. The atomic contact energy provides an

bioRxiv preprint doi: https://doi.org/10.1101/338269; this version posted June 4, 2018. The copyright holder for this preprint (which was not certified by peer review) is the author/funder, who has granted bioRxiv a license to display the preprint in perpetuity. It is made available under aCC-BY 4.0 International license.

estimation of the free energy of the protein interactions. The lower ACE configuration suggests lower free energy, which is more favourable for the formation of pentameric structure [65]. Therefore, the pentameric assembly can be achieved by monomer and dimer intermediates [66]. Using Accelrys Discovery Studio 2.5. with Connelly-type modelling, the relative solvent accessible surface areas (SASA) in the pentameric structure of coat protein could be clearly figured out. In figure 6C, it shows that the predicted solvent accessible surface, which is described in two colours (red and blue), helps in the identification of buried and exposed residues. The results shows that there are hydrophilic residues covers the entire outer region of capsomers and the hydrophobic regions are found in the deep core region.

Analysis of binding sites and surface functional groups for bioconjugation

Three different binding sites were predicted using Molsoft ICM-Pro. The residues I14 (Isoleucine), V60 (Valine) and E78 (Glutamic acid) constitute the members of the binding site of the pentameric protein structure (Figure 7A). These functional groups are identified as being responsible for the formation of multimeric protein structure from the monomers. The surface groups were less polar compared to the accessible or the buried surface but they mostly contain charged residues. It is clear from the surface groups that non-polar interactions (van der Waals and hydrophobic) and polar interactions (hydrogen bond) present at the interfaces between the coat protein subunits are responsible for the assembly of the pentameric form into the capsomere [66]. In addition, Molsoft ICM-Pro has predicted nine different residues occupied on the outer region of the capsid protein. These residues are Lysine (K169), Tyrosine (Y176, 251), Aspartic acid (D82,151), Glutamic acid (E215,220,224), Glycine (G98,147), Asparagine (N157,170), Arginine (R91,144), Valine (V155), and Threonine (T99) (Figure 7B). These residues are the functional groups responsible for the interaction with other molecules.

bioRxiv preprint doi: https://doi.org/10.1101/338269; this version posted June 4, 2018. The copyright holder for this preprint (which was not certified by peer review) is the author/funder, who has granted bioRxiv a license to display the preprint in perpetuity. It is made available under aCC-BY 4.0 International license.

Biocompatibility of expressed SLCCNV coat protein

The MTT assay method is widely used for testing biocompatibility and it provides the quantitative assessment of *in vitro* cell proliferation related to compatible materials. This prerequisite treatment method will be performed to test the potential compatibility issues of *Pichia* expressed SLCCNV-CP in future clinical trials. Therefore, in this *in vitro* assay, after 24 hours of incubation with SLCCNV-CP at thirty concentrations between 0.54 and 18 µg/ml, only viable cells which were capable of metabolizing MTT produced a purple coloured precipitate further analyzed by spectrophotometrically. After 24 hours of incubation, A549 lung cancer cells showed excellent viability against the SLCCNV-CP even up to the concentration of 18µg/ml (Figure 8). The IC_{50} values exceeded 18µg/ml. Significantly, the data showed that the toxicity cut-off range (70%) was reached at a protein concentration of 11µg/ml. It means that up to a concentration of 11µg/ml, SLCCNV-CP is relatively non-toxic to cells. The toxicity testing also helps to calculate the No Observed Adverse Effect Level (NOAEL) dose and is helpful in any further clinical studies [67].

Encapsulation efficiency of SLCCNV-CP-Nanocargo

In this approach, SLCCNV-CP monomers were mixed with MNPs at disassembly buffer (pH 6) and then dialyzed against assembly buffer (pH7). This showed prominent results after analysis through UV-Vis spectroscopy, gel electrophoresis and HRTEM. Figure 9A, the UV-Vis extinction spectra strongly represent the SLCCNV-CP monomers assembled and encapsulated around the magnetic nanoparticles core. However, the original extinction peak for unmodified MNPs changed to a low-intensity peak when encapsulated with SLCCNV-CP monomers, which was reflected by the strong difference in the extinction peak. This reversible change in the

bioRxiv preprint doi: https://doi.org/10.1101/338269; this version posted June 4, 2018. The copyright holder for this preprint (which was not certified by peer review) is the author/funder, who has granted bioRxiv a license to display the preprint in perpetuity. It is made available under aCC-BY 4.0 International license.

583 extinction spectrum clearly demonstrates that the MNPs are stabilized and might be dispersed by
584 the particle in solution. That condition is entirely due to decreased photon absorption by
585 SLCCNV-CP-nanocargo with MNPs. Encapsulation also confirmed at protein gel
586 electrophoresis without staining. In Figure 9B lane 1, the visible band shows that the control
587 unmodified MNPs were not separated. Figure 9B lane 2 shows three visible bands–one band
588 similar to unmodified MNPs and the other two separated in the middle and bottom of the gel.
589 Both bands resulted by the SLCCNV-CP-encapsulated MNPs, which because of the
590 encapuslated protein helps the separation of SLCCNV-CP-MNPs electrophoretically in the gel.
591 However, the band in the middle of the gel may resulted by few MNP particles encapsulated by
592 SLCCNV-CP at a time, which decreased the mobility of SLCCNV-CP and kept them in the
593 middle of the gel. The band in the bottom may be resulted by an individual particle encapsulated
594 by SLCCNV-CP, which has increased the mobility of the SLCCNV-CP-MNPs. In figure 9C-D,
595 HRTEM images (inset), we observed significant differences between the unmodified and
596 SLCCNV-encapsulated MNPs. It clearly indicates that unmodified MNPs were in aggregated
597 state while SLCCNV-CP-encapsulated MNPs were in a dispersed state. In such a case,
598 encapsulated MNPs can be separated by a simple centrifugation method [68]. The EDX analysis
599 also detected higher counts of C,N,O and H atoms in encapsulated MNPs, which corresponds to
600 the atomic complexity of proteins. No such atom counts were observed in unmodified MNPs
601 (Figure 9C-D). A scheme of SLCCNV-CP encapsulation is briefly summarized in Figure 10.
602

603 # Discussions

604 A key challenge in the biomedical field is the development of a smart delivery vehicle with an
605 ability to selectively entrap therapeutic and imaging molecules and display multiple

bioRxiv preprint doi: https://doi.org/10.1101/338269; this version posted June 4, 2018. The copyright holder for this preprint (which was not certified by peer review) is the author/funder, who has granted bioRxiv a license to display the preprint in perpetuity. It is made available under aCC-BY 4.0 International license.

606 functionalities with nanoscale precision. This challenge was overcome successfully by
607 manipulating a plant pathogenic virus to useful scaffolds in the field of biomedical
608 nanotechnology. Here, we chose to study the self-assembling properties of *Squash leaf curl*
609 *China virus* (SLCCNV) of both native whole virus and *Pichia*-expressed virus coat protein
610 monomers. For the first time ever, complete SLCCNV-CP monomeric identical subunits of
611 *Squash leaf curl China virus* (SLCCNV) were successfully expressed through a heterologous
612 expression system using methylotrophic yeast *Pichia pastoris*. In our study, the usual problem
613 associated with prokaryotic expression at post-translational modification for virus proteins
614 (insoluble proteins) was overcome by *Pichia* expression system[19, 20]. By using pPICZαA
615 vector specific to the secretion expression, a protein of our interest was easily isolated from the
616 culture medium by simple centrifugation at 10,000rpm for ten minutes. As a result of these, it
617 was easier to purify the coat protein by ion-exchange chromatography (IEC) after ammonium
618 sulfate precipitation (Figure S3). IEC facilitates the purification of SLCCNV-CP at their pKa
619 values. The IEC can be switched between charged and neutral depending on the pH. It was able
620 to purify the expressed protein without any fusion proteins which might affect the homogeneity
621 of the virus protein. Thus, using heterologous expression yields a high titer of SLCCNV-CP
622 (0.57mg/ml) in the end compared to ultracentrifugation-purified native or native virus proteins
623 (0.241mg/ml) (Figure S2). The sensitivity and specificity of *Begomovirus* coat protein detection
624 was high in the Western blot analysis using polyclonal ACMV antibody. It also meant that the
625 expressed virus proteins were properly refolded and that they retained their antigenic properties,
626 (antigenicity) which was confirmed by the antibody's affinity to the epitope of the coat protein.
627 The identification of *Pichia*-expressed SLCCNV coat protein through MALDI-TOF peptide
628 mass fingerprinting (PMF) showed a significant similarity with other *Begomovirus* species when

bioRxiv preprint doi: https://doi.org/10.1101/338269; this version posted June 4, 2018. The copyright holder for this preprint (which was not certified by peer review) is the author/funder, who has granted bioRxiv a license to display the preprint in perpetuity. It is made available under aCC-BY 4.0 International license.

analyzed through Mascot database searching. It was found to be quite similar to other *Begomovirus* species like SLCCNV-Thailand strain and *Tomato leaf curl New Delhi virus* (ToLCNDV). And the database search shows that there is a maximum (96%) peptide sequence similarity with the SLCCNV-Thailand strain. MALDI-TOF data could provide valuable insights into the *Begomovirus* coat protein and its key role in pathogenesis for future structural study and comprehensive research. Significantly, we confirmed the isoelectric point (pI) of the coat protein monomer as 10 by the MALDI-TOF analysis for first the time. During SDS-PAGE, we observed a novel feature of the *Begomovirus* capsid structural integrity which has never been reported elsewhere[17]. Denaturing agents can disintegrate viral structural proteins only at a high temperature (85˚C–90˚C), which has been confirmed by denaturing gel electrophoresis and DSC analysis. This feature was also evidenced by the *in silico* analysis, that the 3D structure of coat protein monomer has shown the existence of an abundance of random coil, alpha helix and few beta strand. This ratio in the secondary structure can cause the coat protein to be thermodynamically stable at the standard protein denaturing temperature [69]. Moreover, the native virus particles were tremendously stable during dialysis against both acidic and alkali buffers, as were evidenced by HRTEM and DLS data (Figure 3A-C). It understood that only high temperatures or peptide digestive enzymes of protease (either host or virus origin) can cause the cleavage of virus capsids, making them disassociate [70]. A similar kind of stability of virus particles has been observed and reported previously [8].

This investigation of the self-assembly of *Pichia*-expressed SLCCNV-CP has provided unambiguous evidence that it has an inherent ability to self-assemble in a solution without nucleic acid. This point was revealed after examining the ultrafine structures observed on

bioRxiv preprint doi: https://doi.org/10.1101/338269; this version posted June 4, 2018. The copyright holder for this preprint (which was not certified by peer review) is the author/funder, who has granted bioRxiv a license to display the preprint in perpetuity. It is made available under aCC-BY 4.0 International license.

652 HRTEM images, which were the outcome of the *in vitro* self-assembly of numerous capsomeric
653 proteins into a defined structure (Figure4 &5). In this experiment, the assembly pH buffers are
654 act as a cytosolic buffer system which facilitates an *in vitro* assembly of virus coat protein
655 similar in the natural process.
656
657 The pH must have acted as one of the fundamental driving processes for the coat protein self-
658 assembly by the protonation and deprotonation of amino acids [71]. The data obtained from the
659 *in silico* analysis also very much correlating with the results of pH mediated assembly. However,
660 coat protein structure prediction reveals that the subunits consist of a larger proportion of both
661 random coil and alpha helix, which obviously makes the SLCCNV coat protein much more
662 affinity to a hydrogen atom (H) present in the solutions [72]. Basically, protein systems are
663 inherently capable of forming H-bonds in their main chain and side chain amino acids. These
664 groups can, therefore, tend to be responsive while presenting the protein at the various pH
665 environments, and we are bound to agree with another report by Casper (1963) [73] which
666 pinpoints the key role of pH in protein assembly. He suggests that protons are hydrogen-bonded
667 to carboxyl-carboxylate pairs and that they prevent the normal electrostatic repulsion such
668 groups would have on each other. If the two carboxyl groups were ionized, this repulsion could
669 strain the subunit structure and lead to dissolution. This may account for the great sensitivity of
670 the SLCCNV-CP assembly towards change in pH. Thus, the viral coat protein assembly process
671 was found to be very well synchronized with pH and ionic strength [74, 29]. However, altering
672 the pH from acidic to basic could cause a structural transition of virus coat proteins from an
673 undetermined structure (self-assembled aggregates) into a "Nanocargo"-like structure. Besides,
674 the DLS results were clear examples of this phenomenon of structure-associated conformational

bioRxiv preprint doi: https://doi.org/10.1101/338269; this version posted June 4, 2018. The copyright holder for this preprint (which was not certified by peer review) is the author/funder, who has granted bioRxiv a license to display the preprint in perpetuity. It is made available under aCC-BY 4.0 International license.

675 changes (Figure 4 & 5). Thereby, it can be assumed that the calcium ions also have a significant
676 role in the assembly process next to the pH buffer. There are few studies also available to
677 describing the impact of calcium ions in the virus assembly [20, 30, 49,50]. According to that
678 study, calcium ions reportedly act as a chaperon to specifically bind and bring the coat protein
679 subunits together to assemble like a virion capsid. This statement of the study also proved by our
680 intensive study with the bioinformatics tools of PatchDock and Molsoft ICM-Pro modelling.
681 Using bioinformatics tools we found a particular intermediate amino acid residues constituting
682 the members of the binding site between the coat protein monomers identified as Isoleucine
683 (I14), Valine (V60) and Glutamic acid (E78) (Figure 7A). Both Isoleucine and Valine are
684 hydrophobic branched-chain amino acids (BCAA) having an aliphatic side chain and Glutamic
685 acid is polar hydrophilic and negatively charged by its carboxylic acid side chain. Therefore, it
686 assumed that the available BCAA residues primarily neutral at physiological pH should have
687 aliphatic–aliphatic interactions which are known to be a hydrophobic interaction facilitates
688 interaction between the monomer to a monomer [75].
689 These features also make capsomers are thermodynamically stable and also weak in the
690 ionization of pH variation. The previous studies reveals the features of glutamic acid and its
691 natural affinity on the calcium ion [42,53,76]. The calcium ion affinity on the viral coat protein
692 assembly also discussed by few earlier reports [77,59]. According to their study, the *Satellite*
693 *tobacco necrosis virus* (STNV) was able to assemble in the presence of calcium ions at interfaces
694 between the coat protein subunits. They infer/concluded that incorporation of calcium ions into
695 aspartate and glutamate residues contributed to coordinate the STNV capsid assembly in a proper
696 symmetry. Also some studies cited that incorporation of calcium ions into plant virus capsid is
697 typically observed and thought to be involved in viral assembly [29,30,49,59]. Now it has

bioRxiv preprint doi: https://doi.org/10.1101/338269; this version posted June 4, 2018. The copyright holder for this preprint (which was not certified by peer review) is the author/funder, who has granted bioRxiv a license to display the preprint in perpetuity. It is made available under aCC-BY 4.0 International license.

698 become clear that BCAA residues (I14, V60) and glutamic acid (E78) residues are the
699 intermediates that serve as a principal inter-monomer contact, and these contacts are stabilized
700 by pH and calcium ions. Those intermediate interactions presumably can assemble the
701 monomeric form of tertiary structures with further assembly around the existing protein particle
702 that acts as nucleation point, which resulted in high structural organization of quaternary
703 structure of pentamer that must possess a buried hydrophobic core [78]. Thereby, under
704 physiological conditions similar to the intracellular environment, SLCCNV-CP monomers
705 randomly moved and bound one another by their complementary binding sites, resulting in a
706 novel "Nanocargo"-like structure without the aid of an infectious nucleic acid. From the SASA
707 docking results, it was established that there were no hydrophobic residues exposed in the outer
708 regions of the pentameric structure predicted (Figure 6C). Therefore, solvent accessible
709 hydrophilic residues of possibly positively charged residues of lysine, arginine and histidine
710 might be coordinate with negatively charged nucleic acids can facilitate an error-free assembly
711 of a capsid structure [79]. However, the self-assembly and resultant particle morphology is
712 completely reversible upon variation of pH and the number of capsid proteins present in the
713 reaction solution. Any increase in concentration can cause further aggregation around the
714 existing protein particle aggregation that acts as nucleation point, which contributes to the
715 cooperation effect [80].
716
717 Certainly, there is much demand for ingeniously self-assembled protein as a cargo material for
718 usage in targeted therapeutic delivery [4]. Moreover, protein surface bound amino acid residues
719 are most suitable as bioconjugation sites than chemically modified ones [81].Our self-assembled
720 SLCCNV-CP-Nanocargo are composed of many identical copies of coat protein which consist of

bioRxiv preprint doi: https://doi.org/10.1101/338269; this version posted June 4, 2018. The copyright holder for this preprint (which was not certified by peer review) is the author/funder, who has granted bioRxiv a license to display the preprint in perpetuity. It is made available under aCC-BY 4.0 International license.

amino acid side chains found to be most suitable for bioconjugation than any others previously reported [8].These were predicted by the same Molsoft ICM-Pro bioinformatics tool which has predicted nine potential conjugation sites available on the exterior surface of SLCCNV coat protein monomer such as Lysine, Tyrosine, Aspartic acid, Glutamic acid, Glycine, Asparagine, Arginine, Valine and Threonine (Figure 7B) [81-82]. No free Cysteine side chains predicted which is one of the popular site for the bioconjugation methodology. The predicted available side chains, particularly amine group containing Lys, carboxylate group containing Asp then Glu, aromatic group containing Tyr are the most common bioconjugation residues utilized for the conjugation chemistry for a stable covalent link between molecules [8]. Moreover, they are the groups predominantly available on the surface of the pentameric coat protein structure. The remaining amino acids Gly, Asp, Arg, Val, and Thr are used as alternatives and specifically to tether the molecules via ionic and hydrophobic interactions with chemical intermediates. These are the residues of functional groups responsible for the interaction of the protein with other molecules [81-82]. In this regard, SLCCNV-CP-Nanocargo can be functionally modified with any kind of molecules to become "smart hybrid materials" for potential applications. It is also possible to encapsulate any small molecules (either polar or non-polar), in a single step by SLCCNV-CP-Nanocargos [8]. Their efficiency would be directed by the concentration and the relative ratio between SLCCNV coat protein and specific molecules, making them one of the finest virus hybrid materials. An important question that we have the answer now is about the biocompatible properties of SLCCNV-"Nanocargo". There are only few studies reported the biocompatible properties of plant virus nanoparticles previously [8]. From the cell cytotoxicity assay, it was strongly determined that using plant virus like particles for furthering any biomedical application studies would be considered safe. The purified SLCCNV-CP has proved

bioRxiv preprint doi: https://doi.org/10.1101/338269; this version posted June 4, 2018. The copyright holder for this preprint (which was not certified by peer review) is the author/funder, who has granted bioRxiv a license to display the preprint in perpetuity. It is made available under aCC-BY 4.0 International license.

744 to be a potential biocompatibility material among the existing classes of protein biomaterials and
745 that it can be used without any modification to enhance the pharmacokinetic properties in the
746 clinical trials. Thus, now we have disclosed all the potential answers for the possible SLCCNV
747 coat protein assembly both experimentally and computationally.
748 Finally, the capability of self-assembled SLCCNV-CP as "Nanocargo" was determined by using
749 magnetic nanoparticles (MNPs) as a core to encapsulate coat protein monomers. Under optimal
750 assembly (pH 7.0 - 8.0) conditions, encapsulation occurs spontaneously by mixing the protein
751 subunits with cargo particles (MNPs) at a detectable level by UV-Vis absorbance, SDS-PAGE,
752 HRTEM and EDX (see figure 16). The absorbance peak variation between free MNPs and coat
753 protein-encapsulated MNPs clearly denotes the possible "Nanocargo" process (figure 16 A).
754 Similarly, the principle of the separation technique of SDS-PAGE separated both free MNPs and
755 coat protein-encapsulated MNPs by size (figure 16 B). The SLCCNV coat protein facilitates the
756 mobility of encapsulated MNP and MNPs electrophoretically. At the HRTEM images, the fine
757 results were observed, which correlated well with other results in this section (figure 16 C & D).
758 This kind of encapsulation initiated via electrostatic interactions of the coat proteins with
759 negatively charged magnetic particles results in SLCCNV-CP as an artificial Nanocargo. It is not
760 surprising, then, that, the *in vitro* reconstitution of such virus coat protein is driven by
761 electrostatic interactions. It is for the same reason that the virus coat protein shows an amazing
762 ability to encapsulate not only its genetic materials but also non-native genetic materials like
763 surface functionalized nanoparticles and other molecules. An understanding of the physical
764 principles underlying the spontaneous encapsulation of negatively charged particles could help
765 realize the envisaged applications in medical imaging and controlled drug release. Now, the
766 objective of this work has helped reach the conclusion that using SLCCNV-CP-Nanocargo,

bioRxiv preprint doi: https://doi.org/10.1101/338269; this version posted June 4, 2018. The copyright holder for this preprint (which was not certified by peer review) is the author/funder, who has granted bioRxiv a license to display the preprint in perpetuity. It is made available under aCC-BY 4.0 International license.

767 encapsulation can be enabled in any other species (genomic or non-genomic) at the specific ionic
768 strengths in the medium.
769
770

771 Conclusions

772 Self-assembling properties of virus capsid proteins is a realistic and attractive material. The virus
773 capsid proteins can advance the development of fabricating a robust nanotools for the
774 nanotechnology application. Hence, we began to manipulate one of the well-known destructive
775 plant pathogenic viruses – *Squash leaf curl China virus* (SLCCNV) – towards self-assembled
776 "Nanocargo"-like virus structures. In this experiment, *Pichia* expressed SLCCNV-CP showed a
777 high affinity towards pH along with calcium ions, which spontaneously facilitated the
778 reformation of monomers to constraint "Nanocargo"-like structures. The resultant SLCCNV-CP-
779 Nanocargo's are stable under a pH similar to physiologic pH, and it can be disassemble simply
780 by changing the pH to acidic. Using this pH-responsive assembly/disassembly mechanism, the
781 magnetic nanoparticles (MNPs) were successfully entrapped into "SLCCNV-CP-Nanocargo"
782 materials. This pH-responsive gating mechanism is a feasible way to accommodate various kinds
783 of therapeutic and diagnostic molecules within the "SLCCNV-CP-Nanocargo", which will
784 address them as a next generation nanotool with promising biomedical applications. In fact, pH-
785 responsive materials are in demand in the area of target therapeutic delivery [83]. For example,
786 this type of pH-responsive reversible materials allows triggered release of therapeutic materials
787 to an acidic environment at the tumour site [84]. Moreover, through a bioinformatics study, we
788 sufficiently gained some realistic information about coat protein assembly, which correlates
789 highly with the results obtained from *the in vitro* experiment. Also, another phase of *in silico*

bioRxiv preprint doi: https://doi.org/10.1101/338269; this version posted June 4, 2018. The copyright holder for this preprint (which was not certified by peer review) is the author/funder, who has granted bioRxiv a license to display the preprint in perpetuity. It is made available under aCC-BY 4.0 International license.

790 analysis deciphered the potential bioconjugation sites available in the SLCCNV-CP which could
791 be work favourably to tether any functional moiety to deliver at the tissue target site.
792 Significantly, it was proved that "SLCCNV-CP-Nanocargo" has no cytotoxic effects in
793 maximum concentrations to mammalian cancer cell lines which can manifest "SLCCNV-CP-
794 Nanocargo" as a potential biocompatibility material. Even though there are hundreds of virus-
795 like particles studied, our extensive studies of the self-assembly of SLCCNV-coat protein show
796 unique features which are very new to viral nanotechnology and which will also throw much
797 light on smart delivery vehicle research in the biomedical field.
798
799
800
801
802

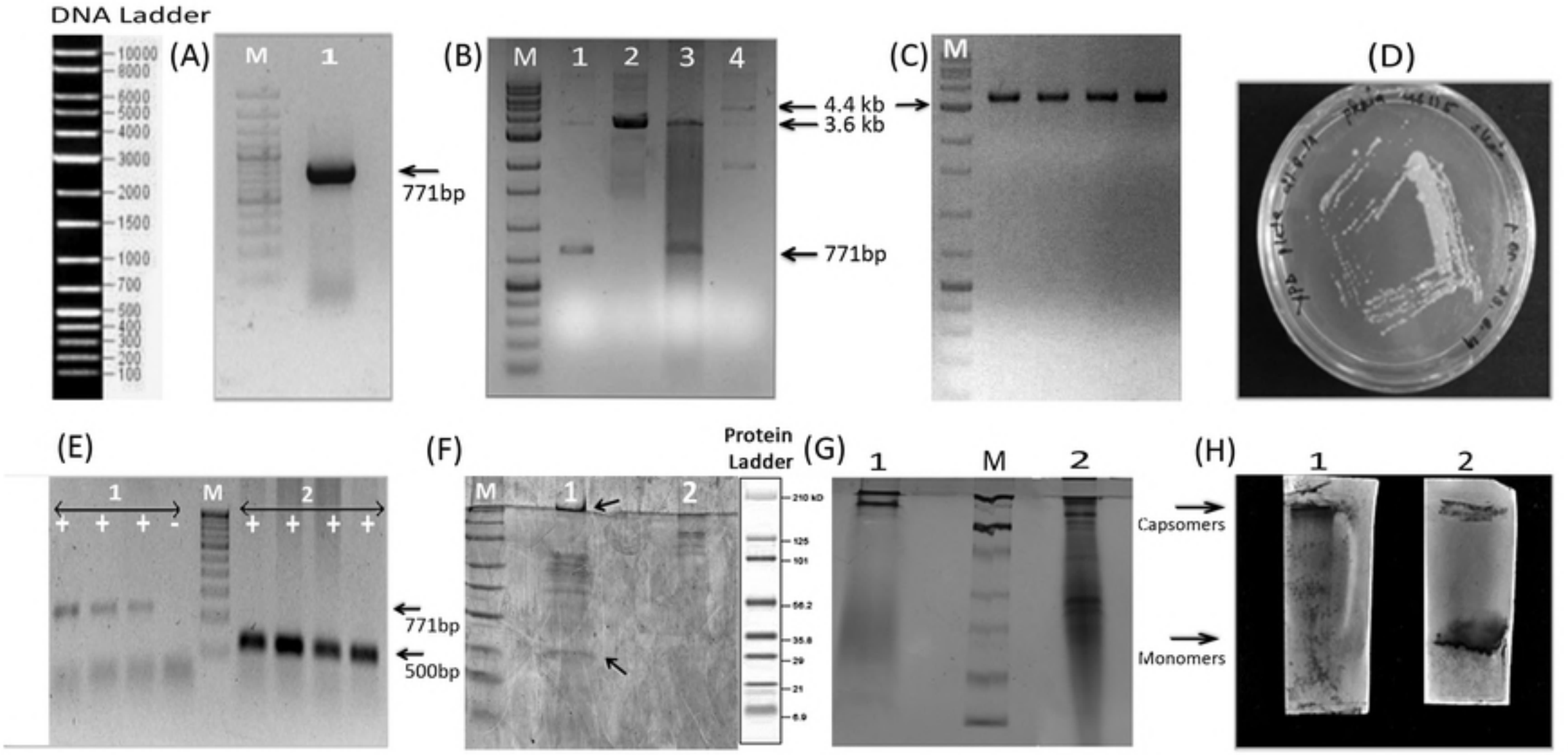
DNA Ladder
10000
8000
6000
5000
4000
3000
2000
1500
1000
700
500
400
300
200
100
(A)
M
1
771bp
(B)
M
1
2
3
4
4.4 kb
3.6 kb
771bp
(C)
M
(D)
(E)
1
M
2
+ + + -
+ + + +
771bp
500bp
(F)
Protein Ladder
M
1
2
210 kD
125
101
56.2
35.8
29
21
6.9
(G)
1
M
2
(H)
1
2
Capsomers
Monomers

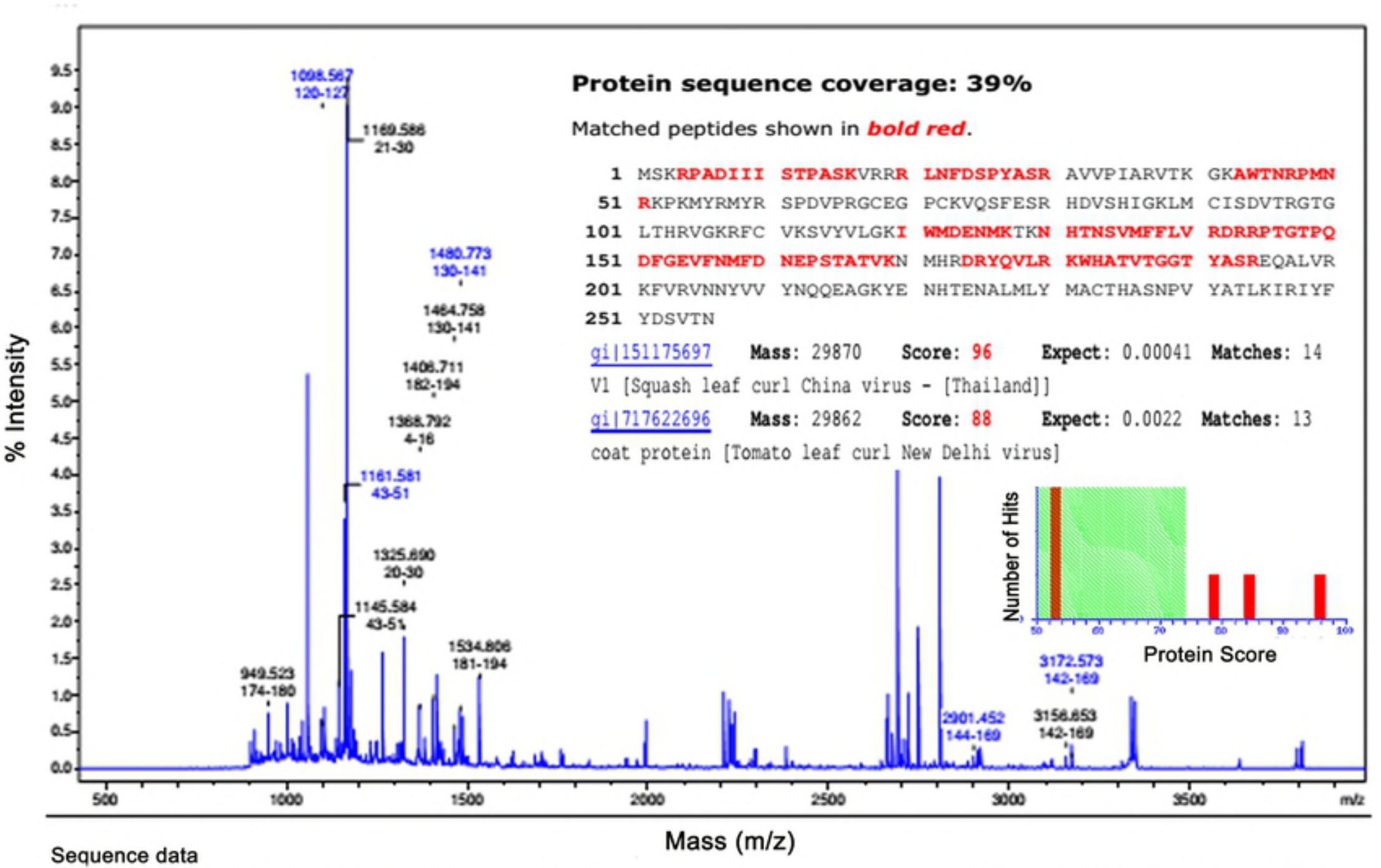

Sequence data

V1 [Squash leaf curl China virus-[Thailand]] gi|1511775697

Intensity Coverage: 46.8% (22093 cnts)

Sequence Covergae MS: 39.8%

pI (Isoelectric point): 10.7

bioRxiv preprint doi: https://doi.org/10.1101/338269; this version posted June 4, 2018. The copyright holder for this preprint (which was not certified by peer review) is the author/funder, who has granted bioRxiv a license to display the preprint in perpetuity. It is made available under aCC-BY 4.0 International license.

(A)

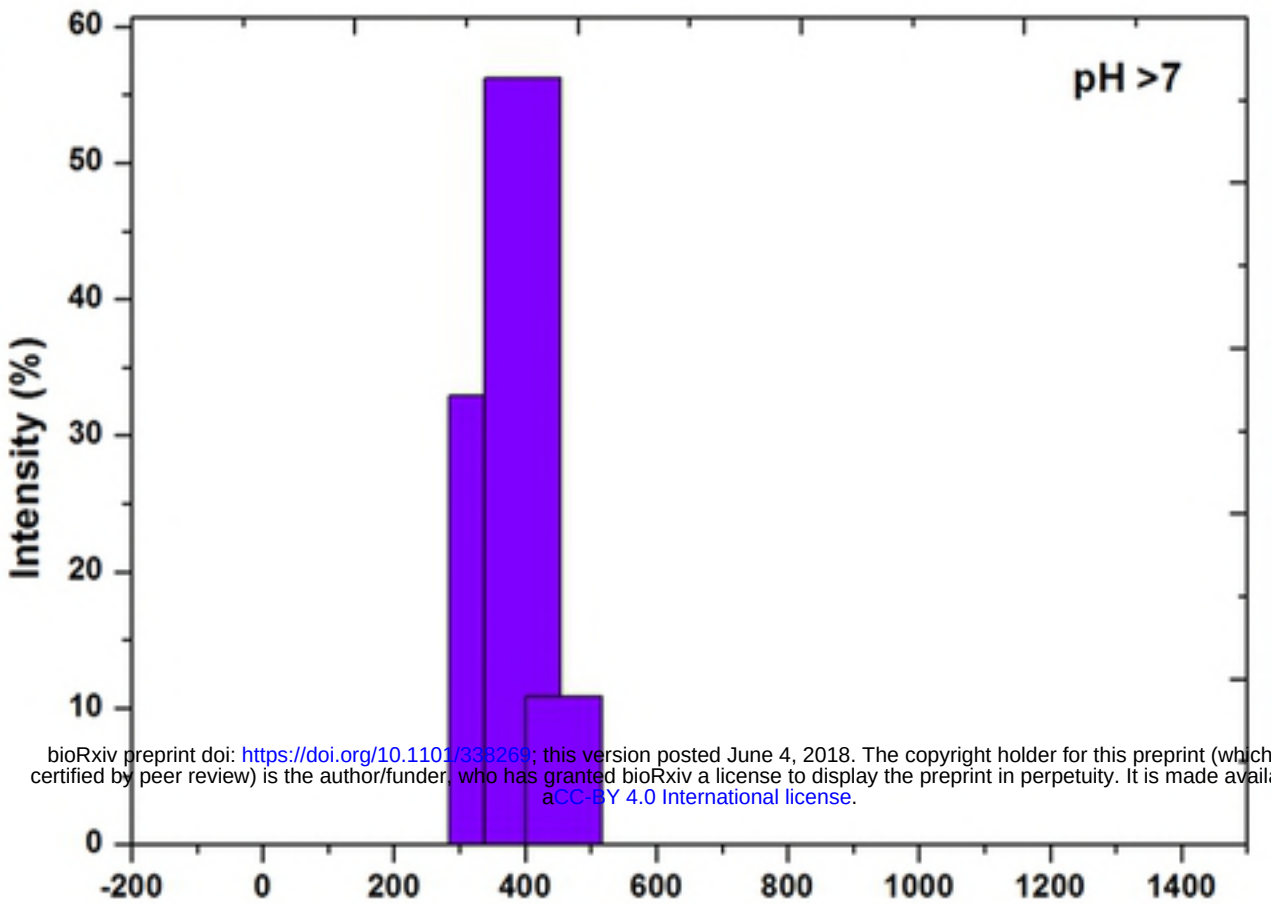

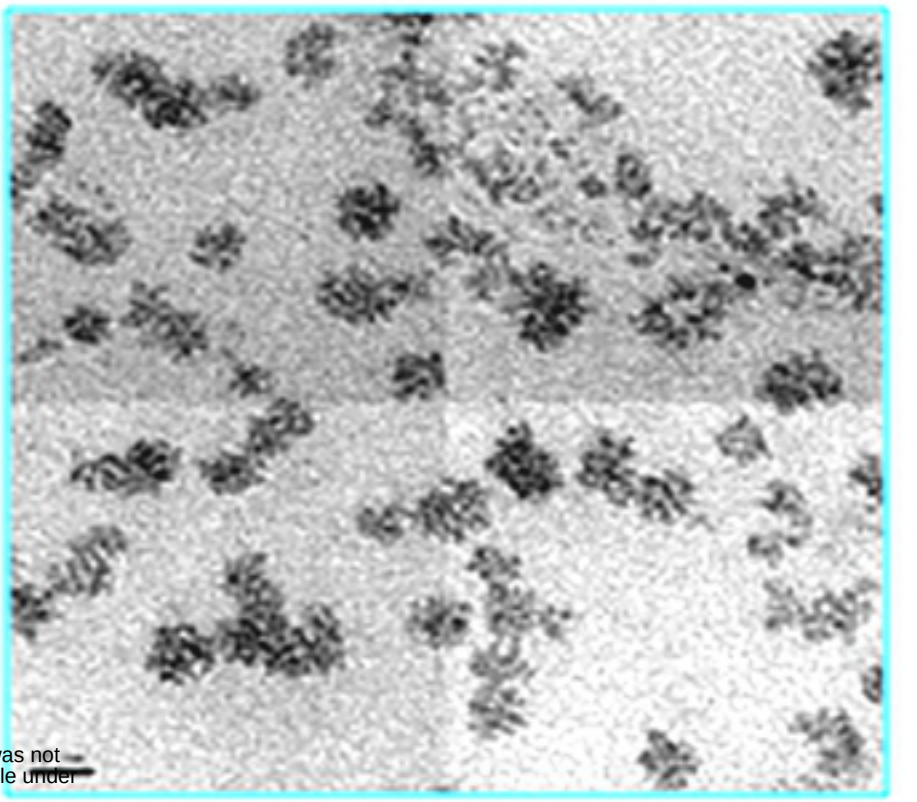

(B)

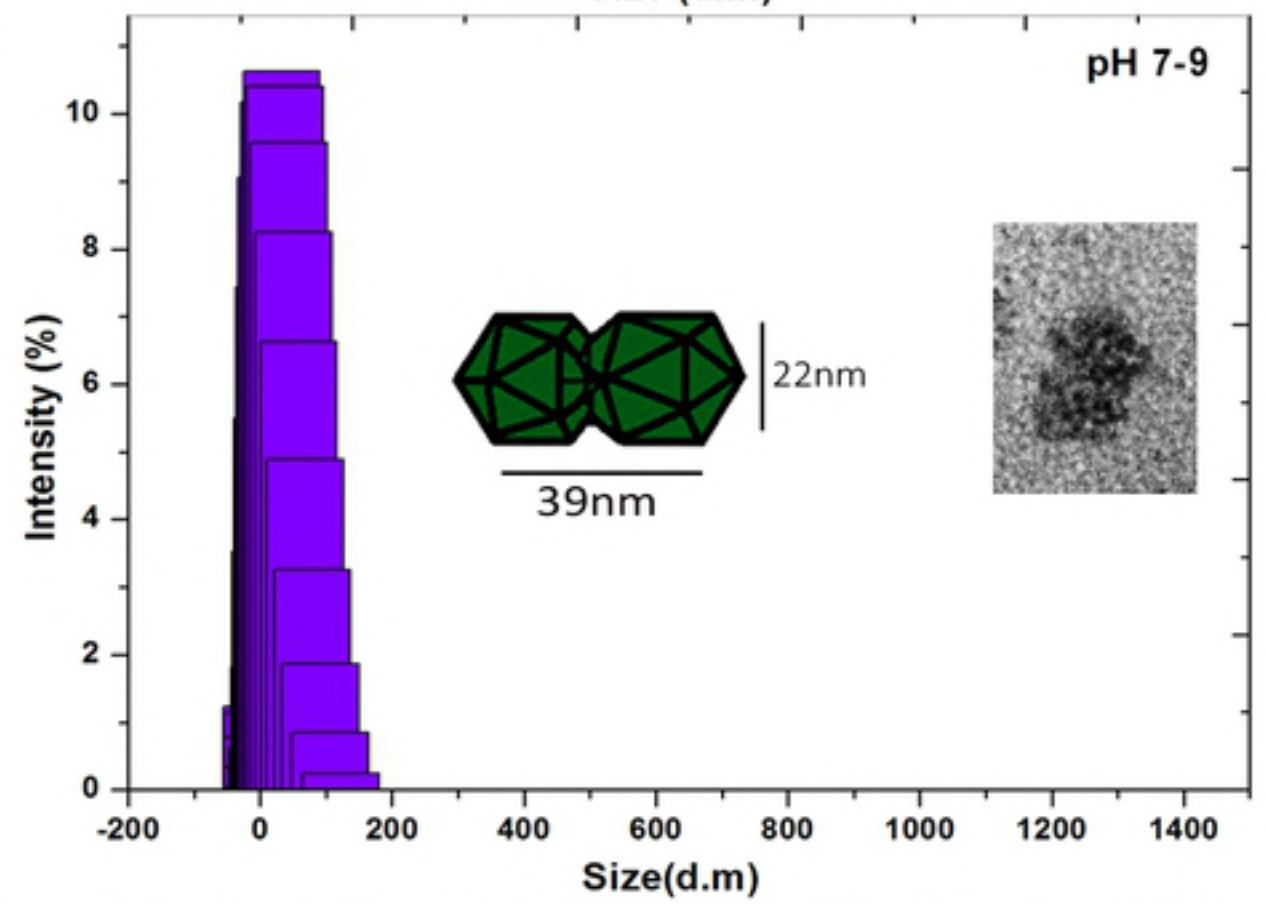

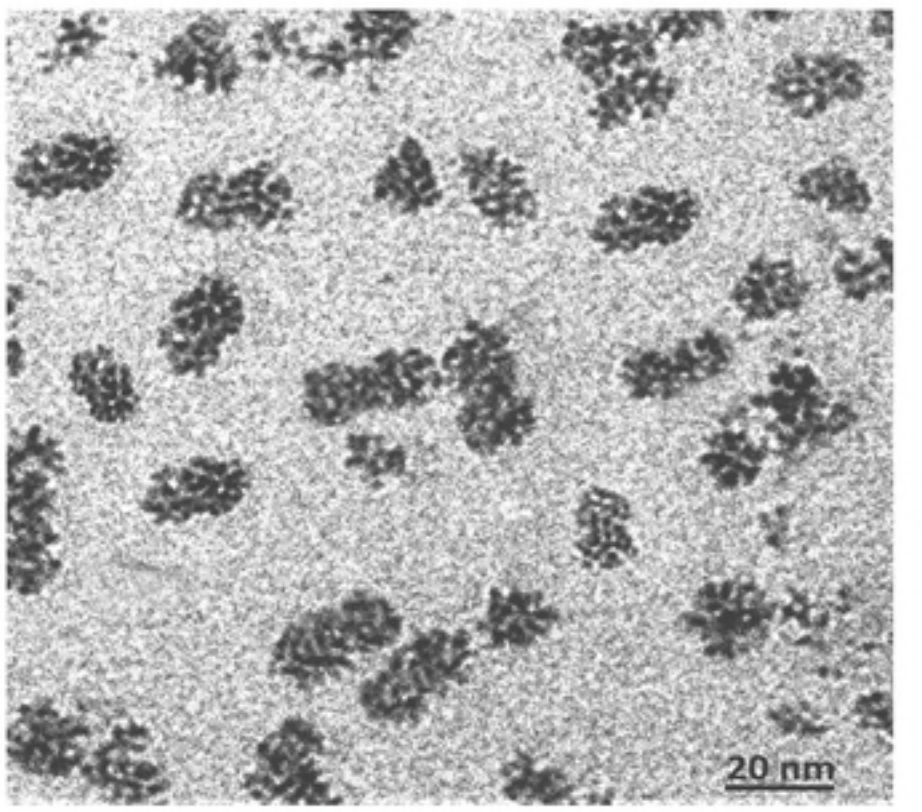

(C)

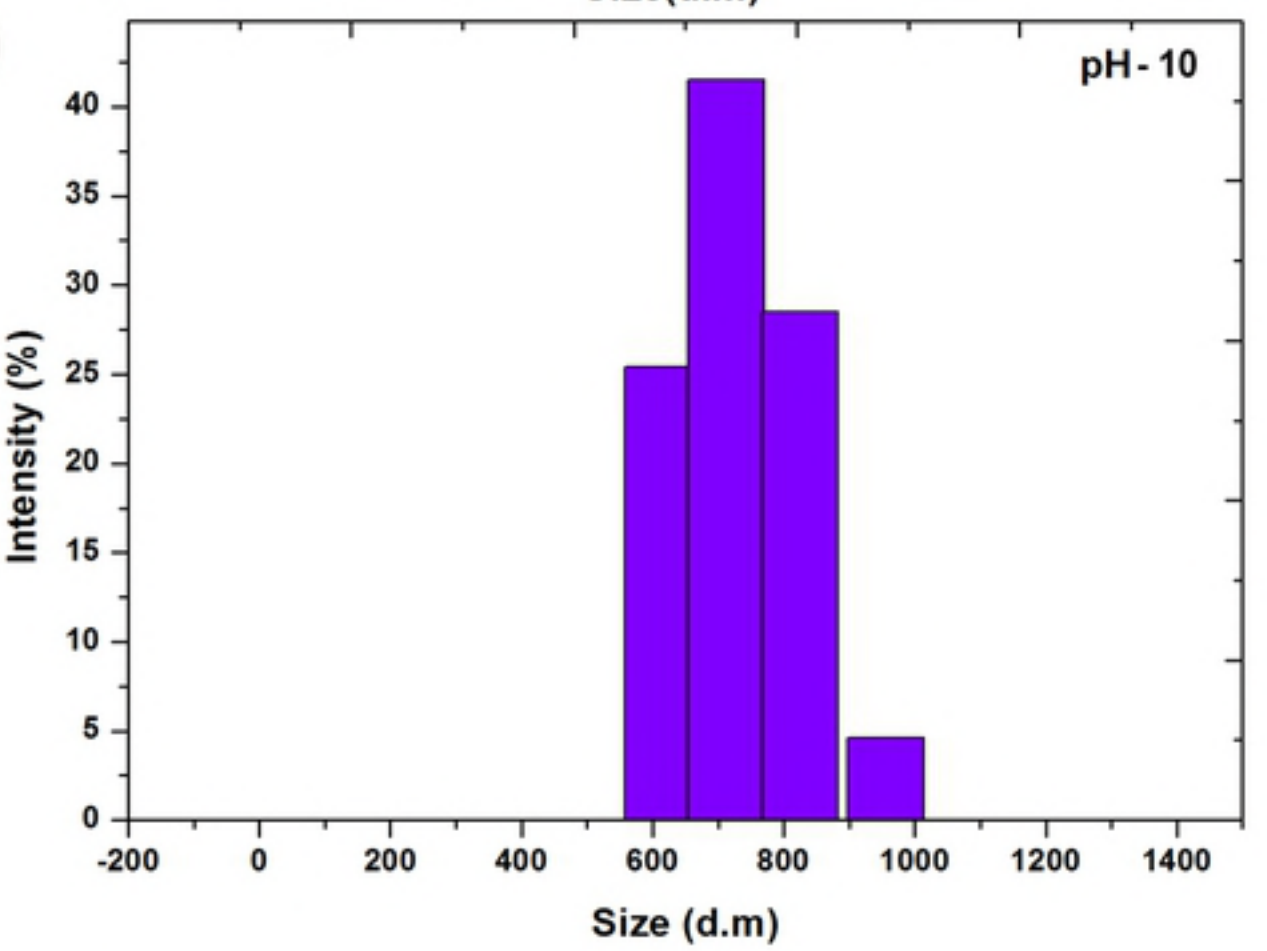

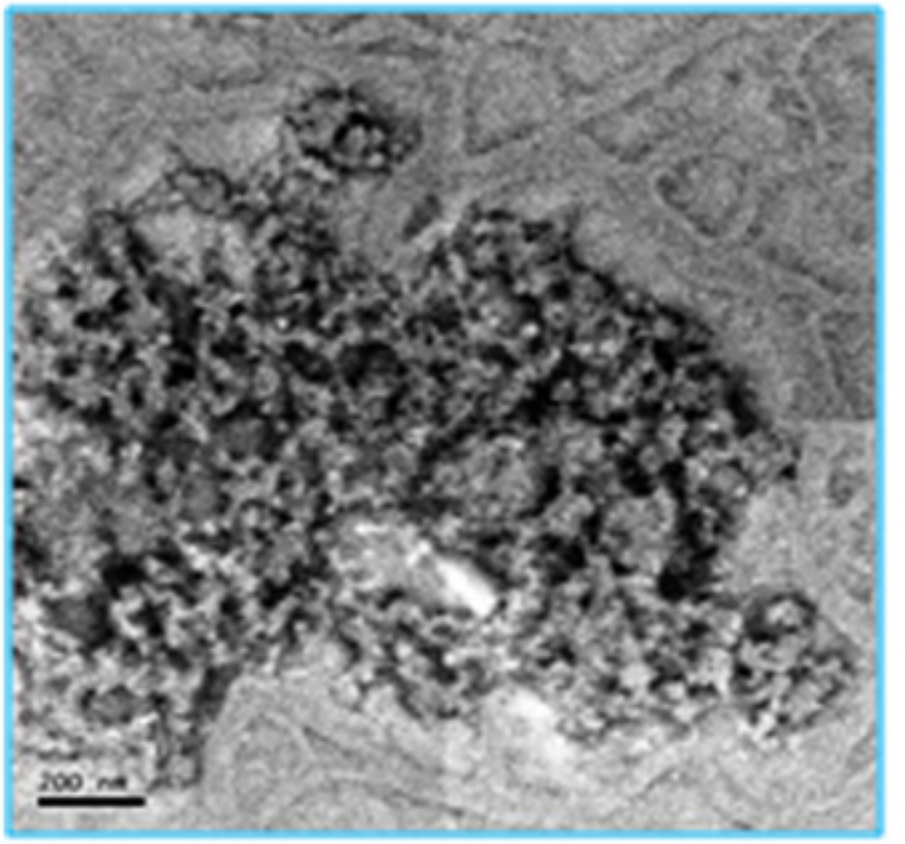

bioRxiv preprint doi: https://doi.org/10.1101/338269; this version posted June 4, 2018. The copyright holder for this preprint (which was not certified by peer review) is the author/funder, who has granted bioRxiv a license to display the preprint in perpetuity. It is made available under aCC-BY 4.0 International license.

(A)

pH 5

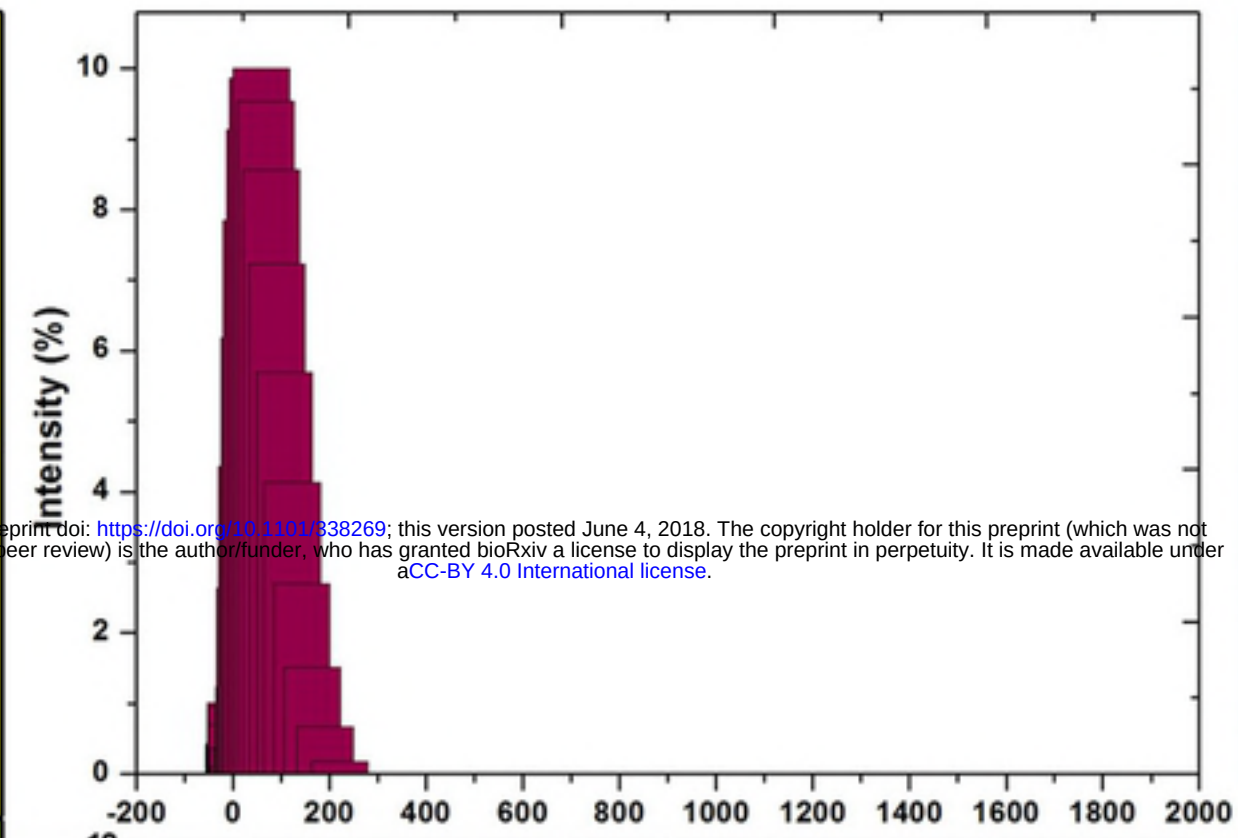

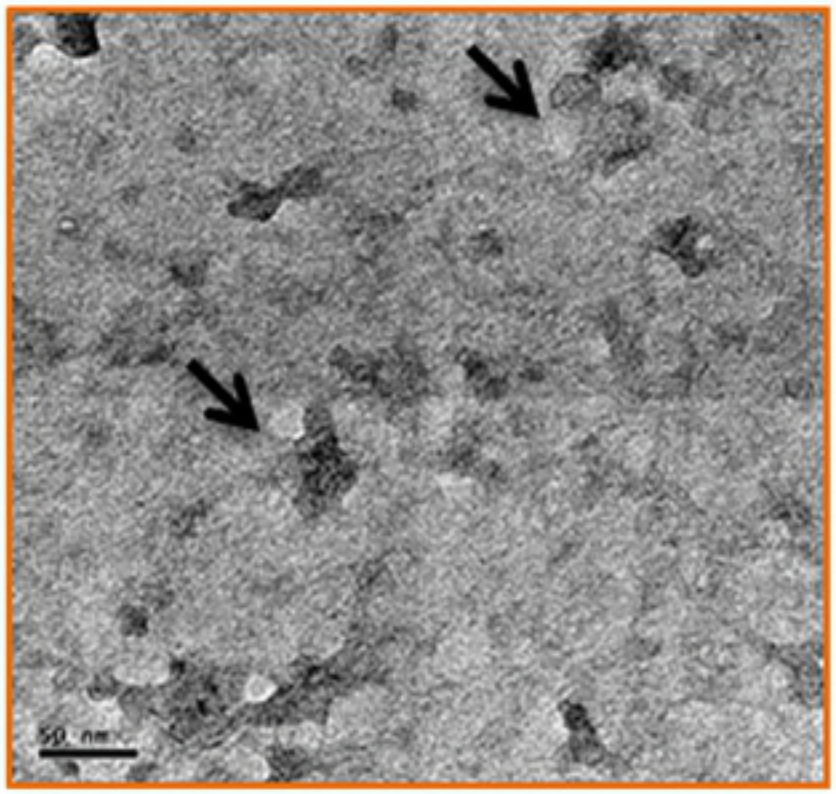

(B)

pH 6

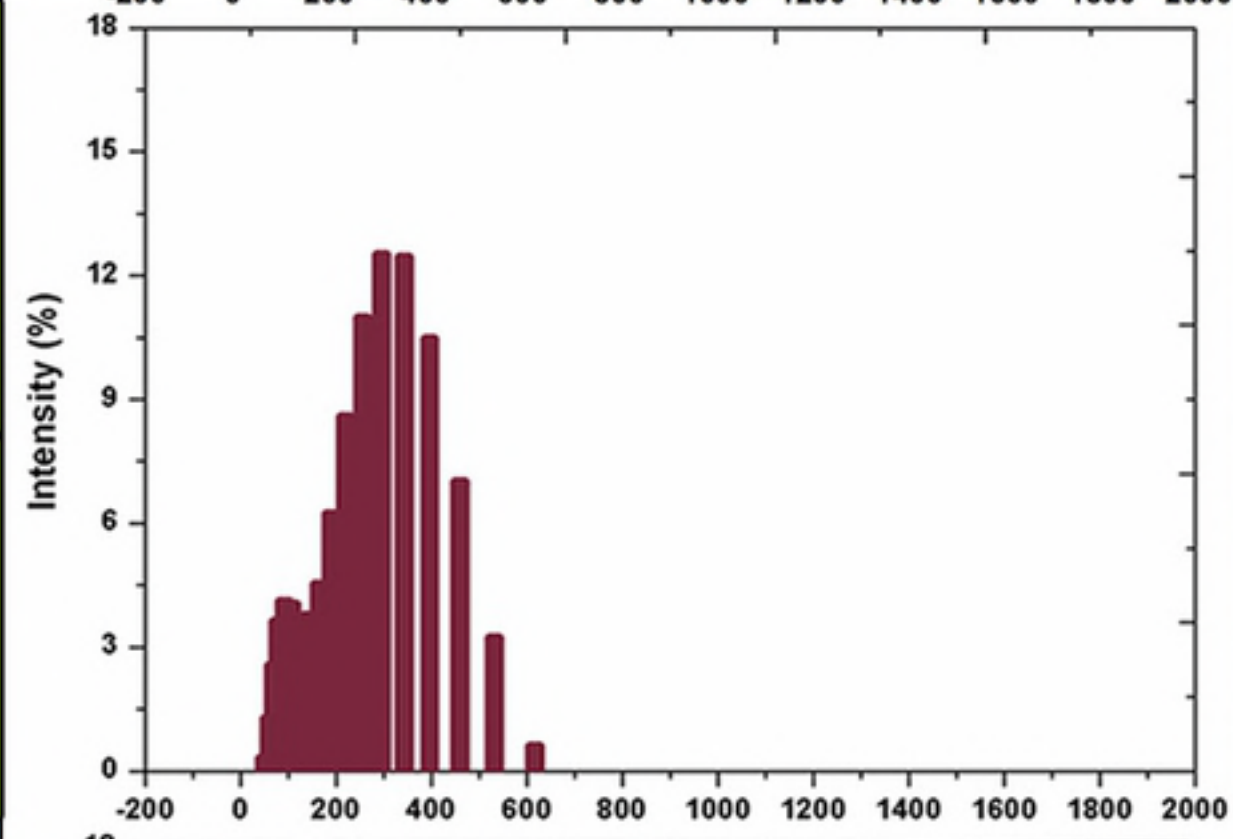

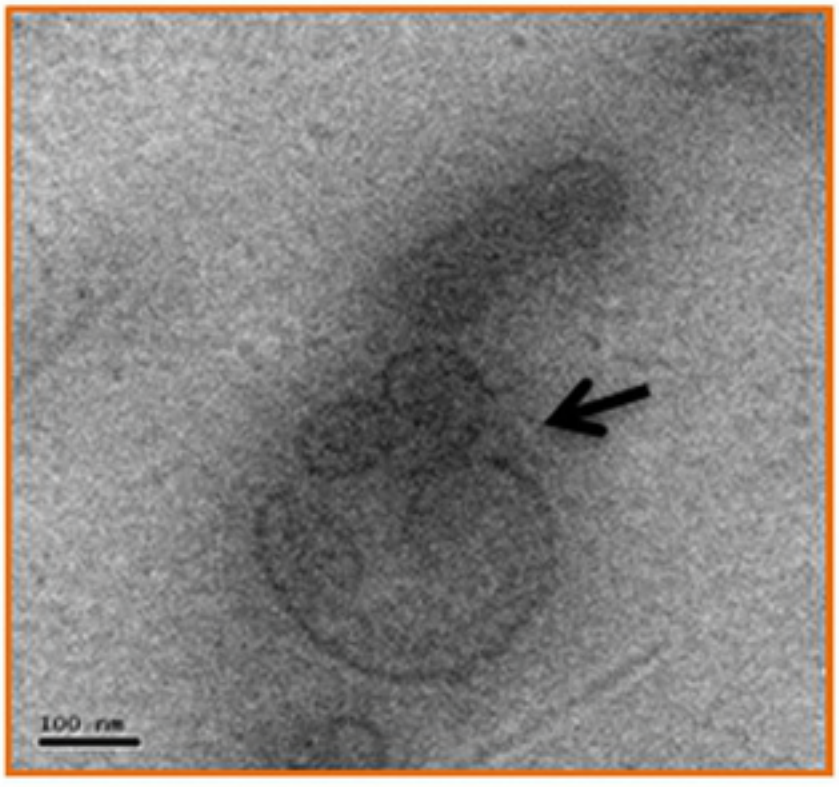

(C)

pH 7

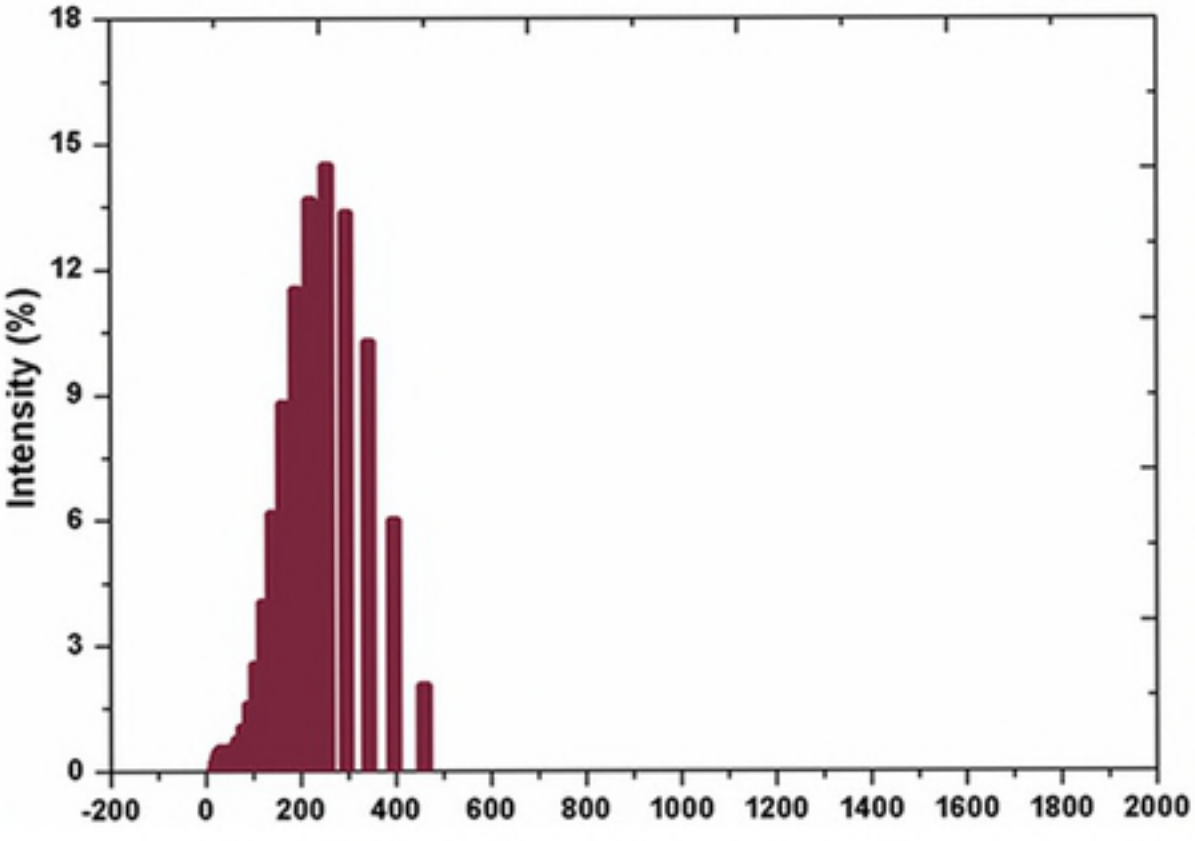

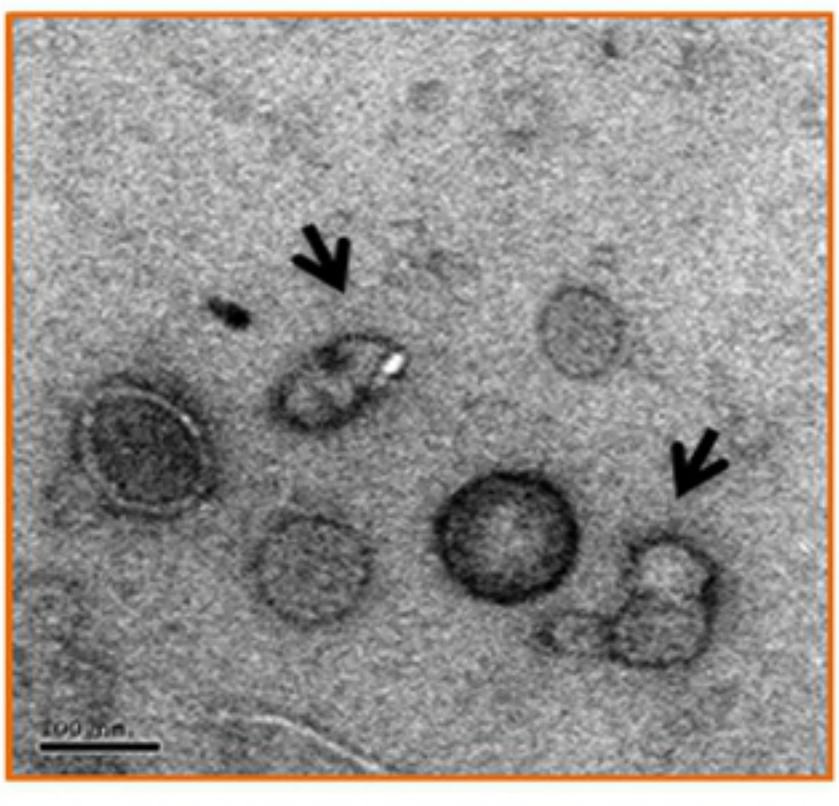

bioRxiv preprint doi: https://doi.org/10.1101/338269; this version posted June 4, 2018. The copyright holder for this preprint (which was not certified by peer review) is the author/funder, who has granted bioRxiv a license to display the preprint in perpetuity. It is made available under aCC-BY 4.0 International license.

(D)

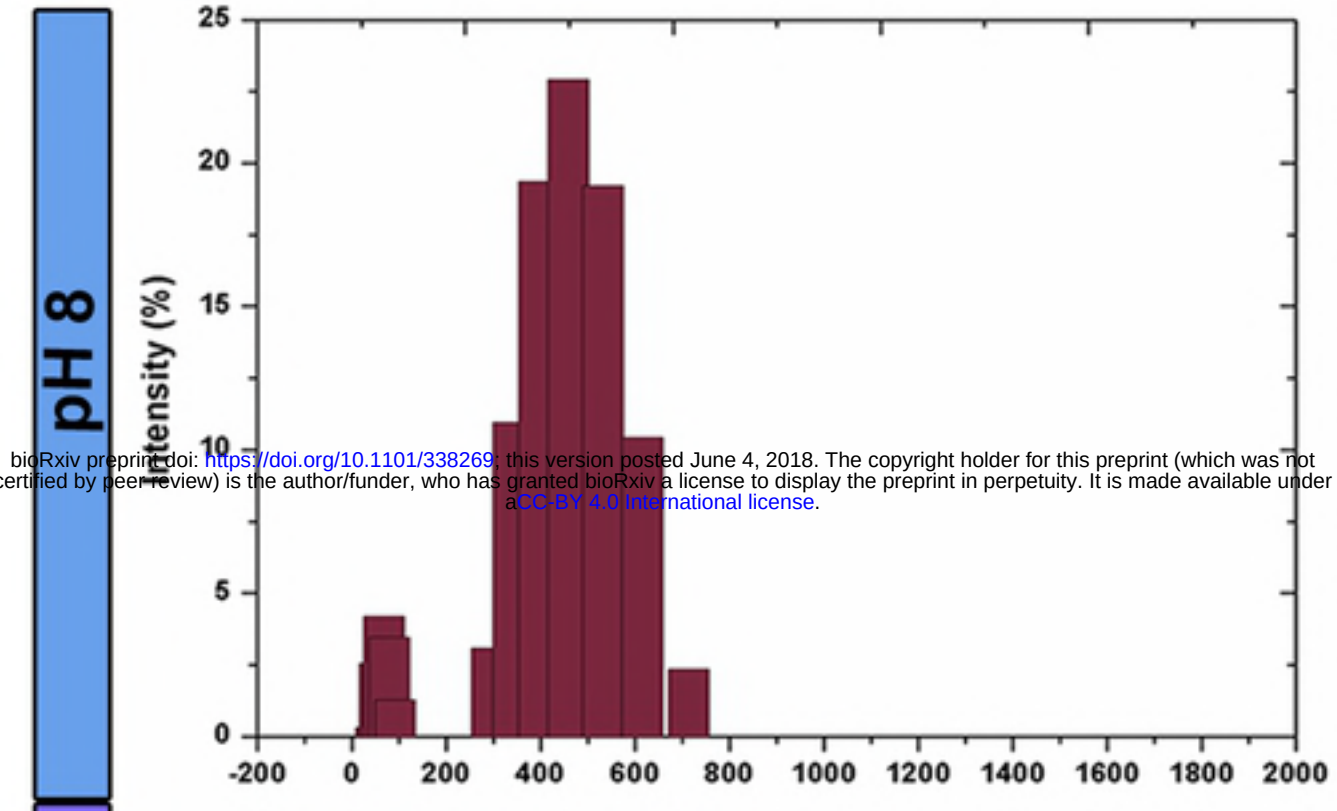

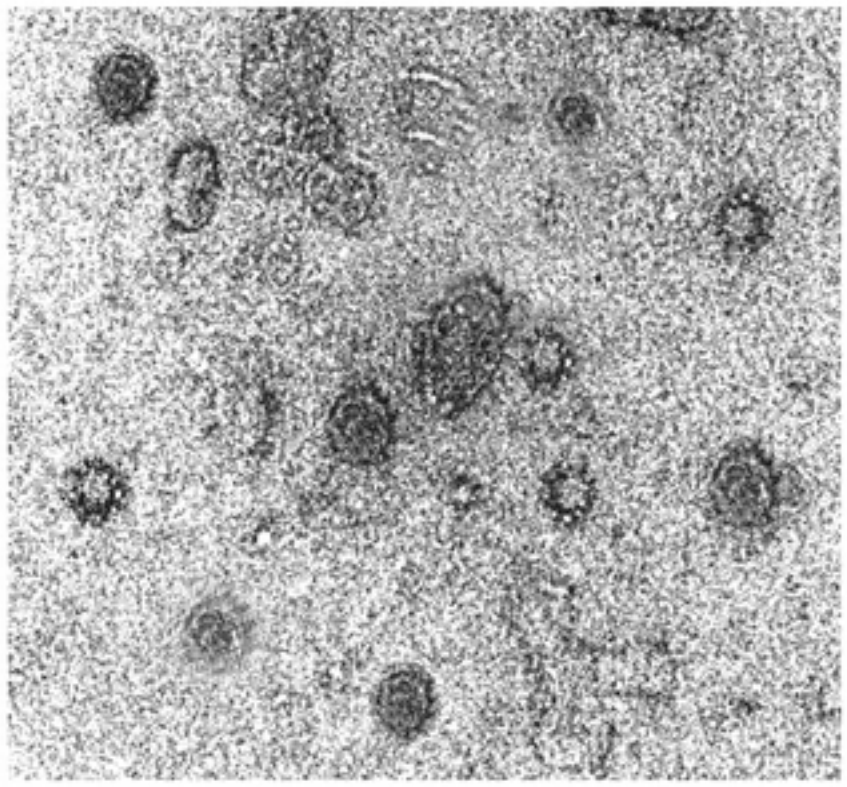

(E)

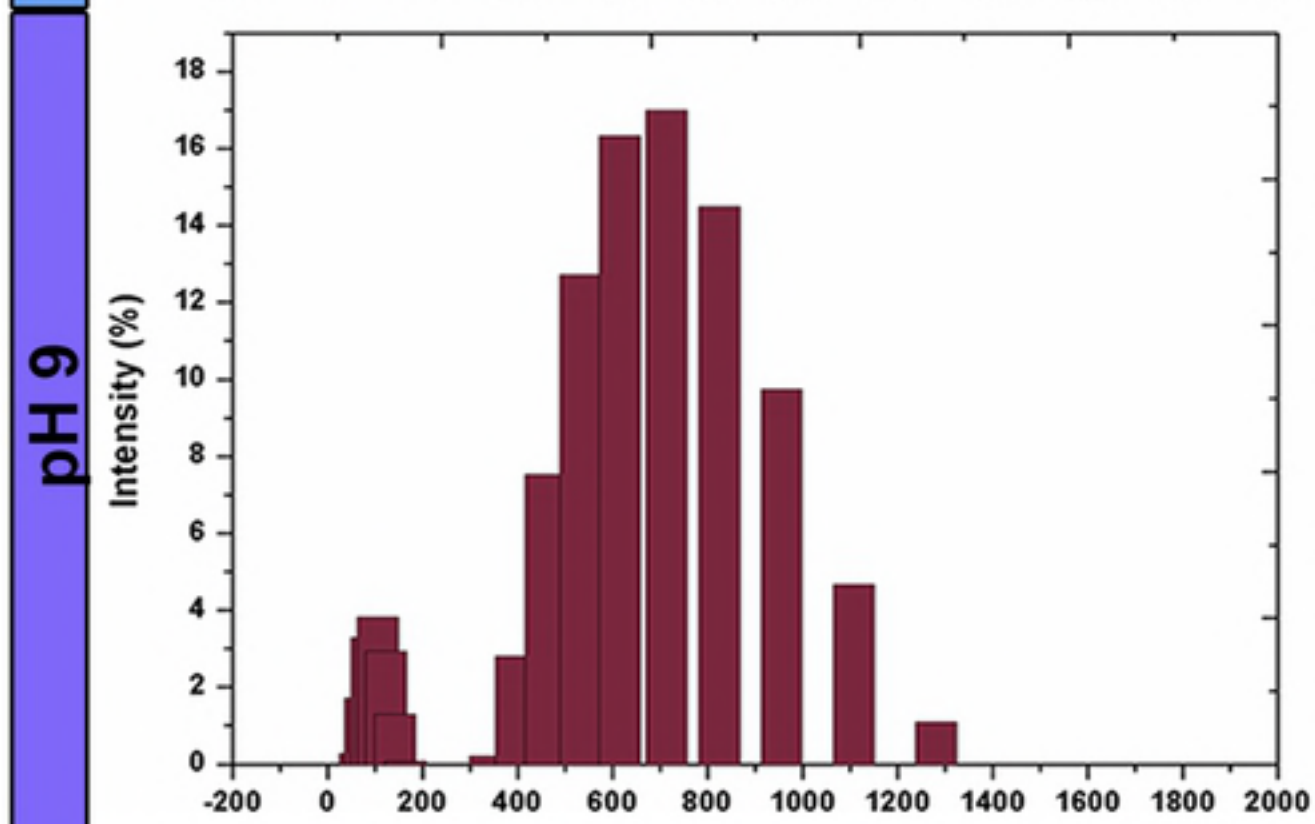

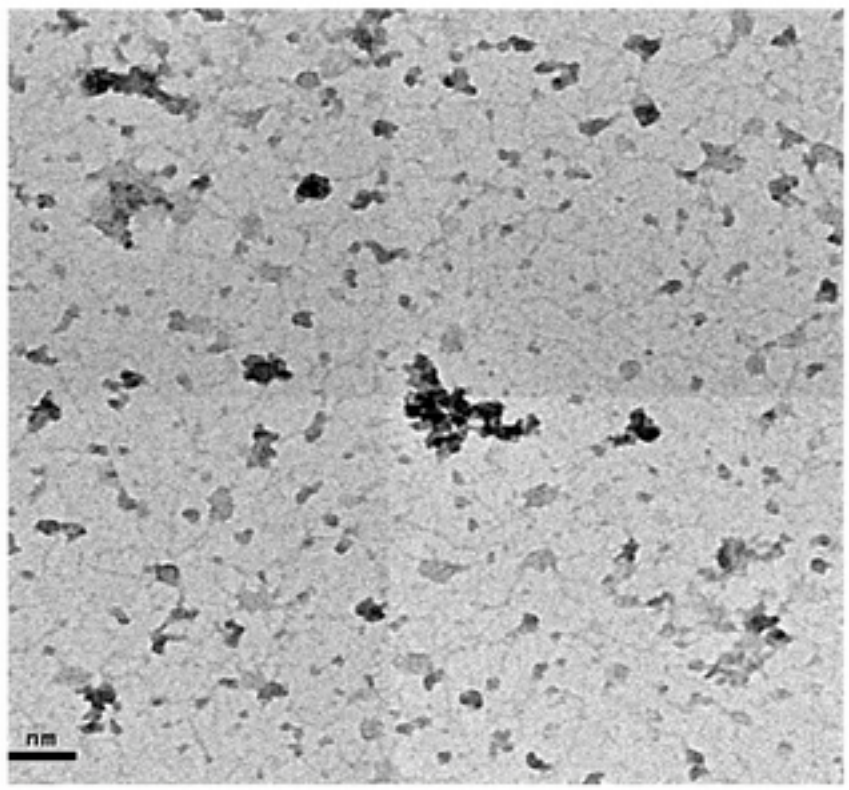

(F)

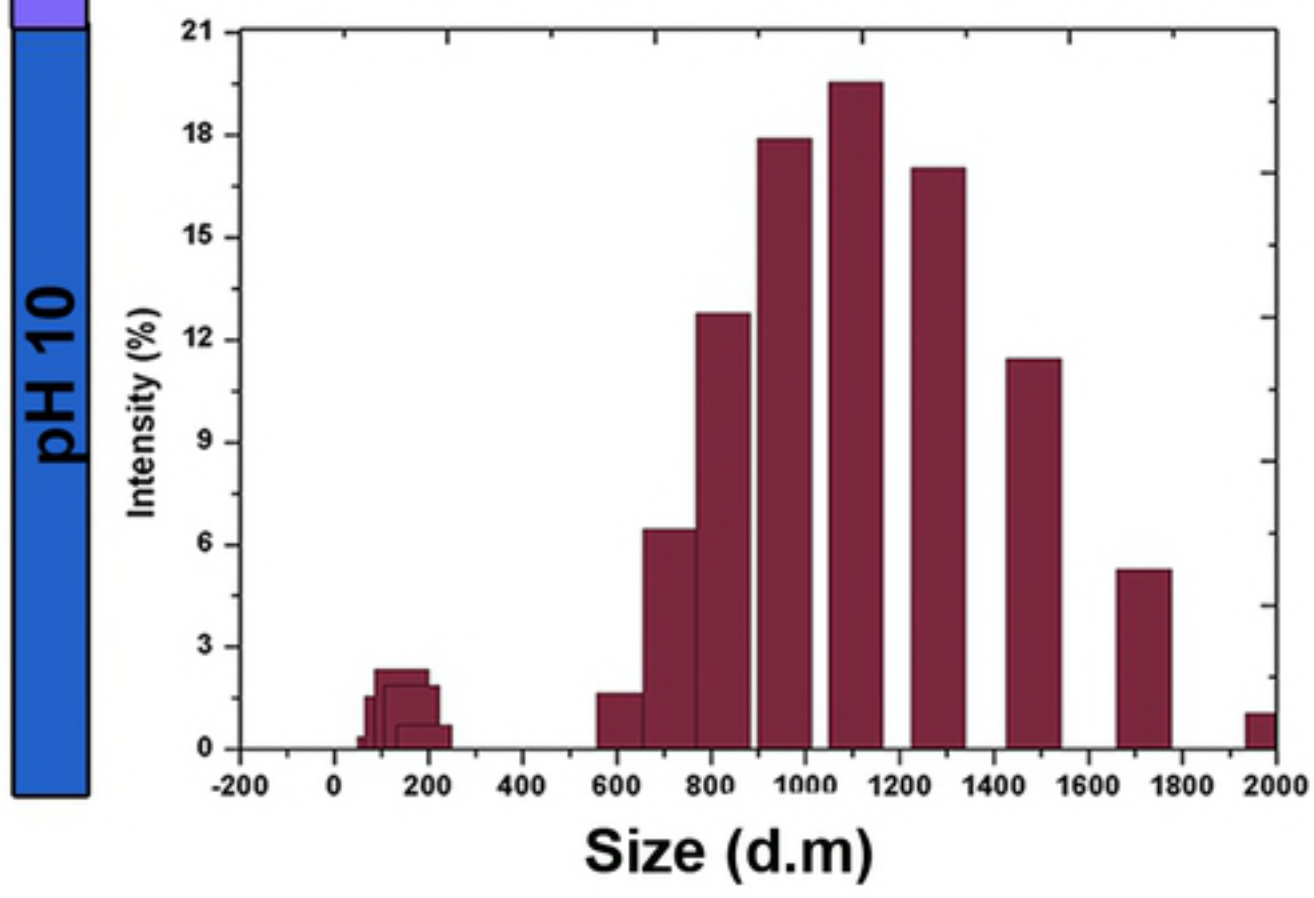

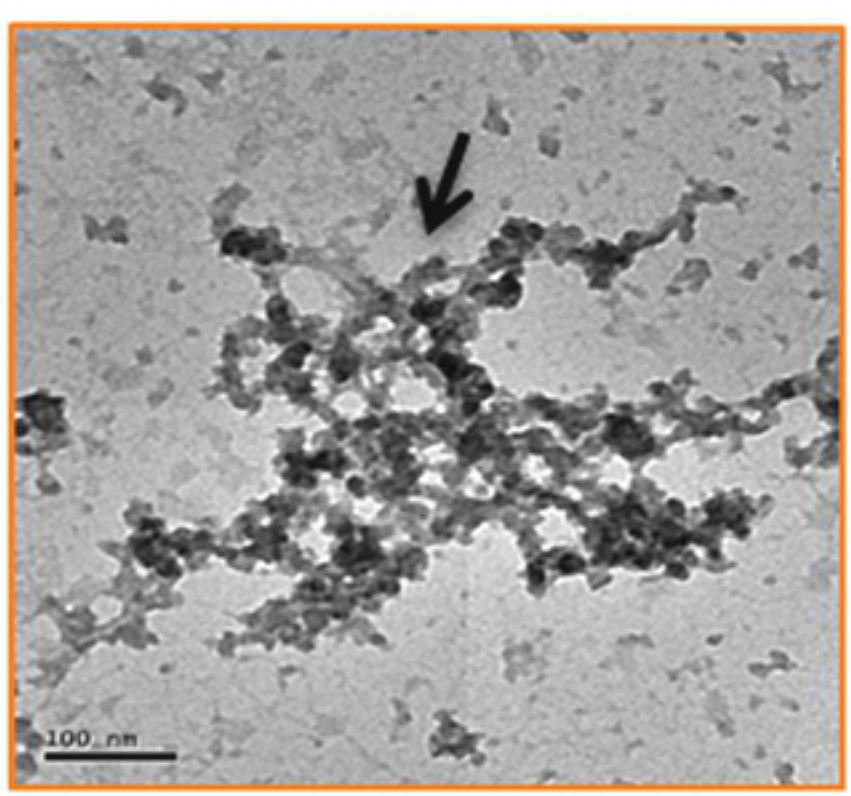

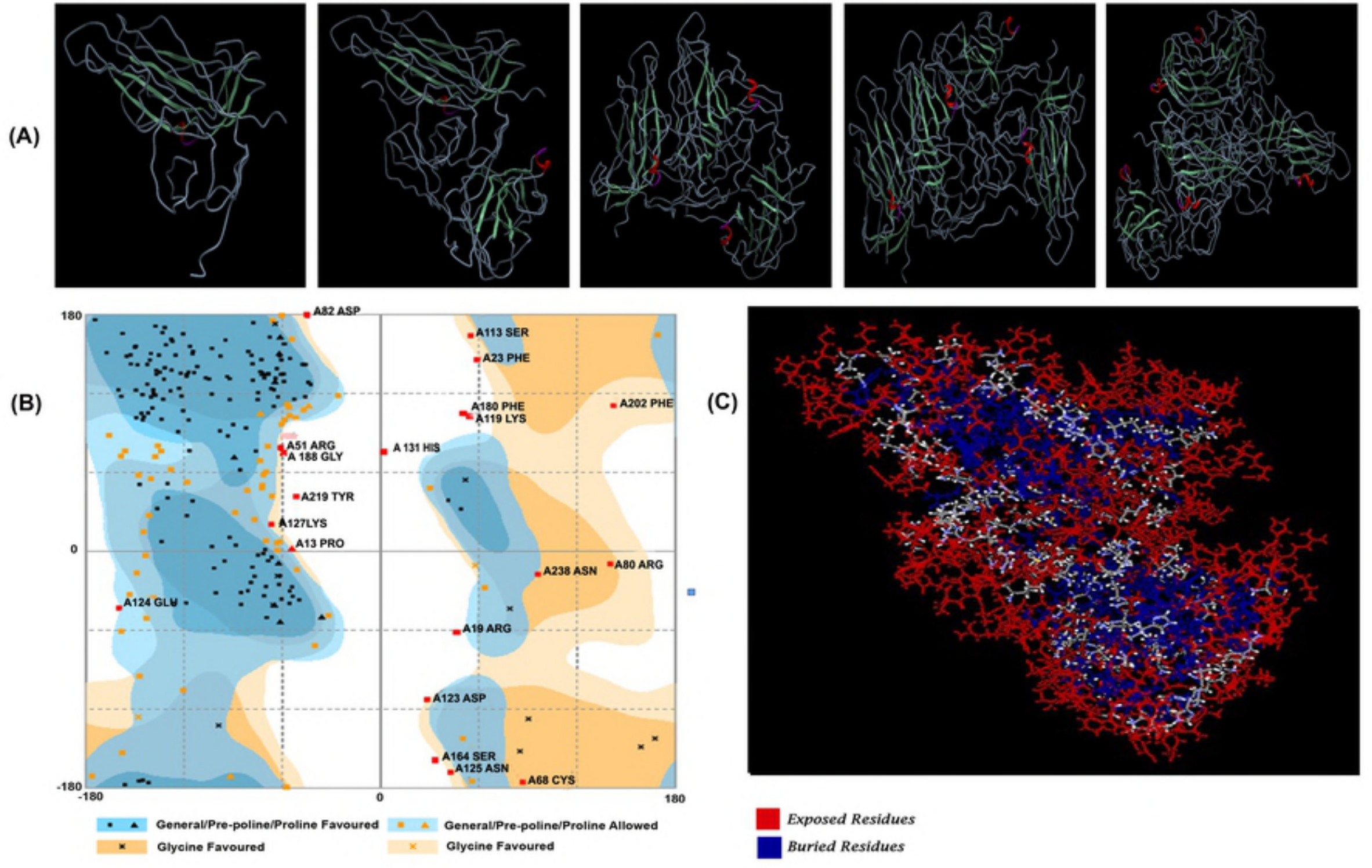
(A)
(B)
(C)
180
0
-180
-180
0
180
A82 ASP
A113 SER
A23 PHE
A180 PHE
A119 LYS
A202 PHE
A51 ARG
A 188 GLY
A 131 HIS
A219 TYR
A127LYS
A13 PRO
A238 ASN
A80 ARG
A124 GLU
A19 ARG
A123 ASP
A164 SER
A125 ASN
A68 CYS
General/Pre-poline/Proline Favoured
Glycine Favoured
General/Pre-poline/Proline Allowed
Glycine Favoured
Exposed Residues
Buried Residues

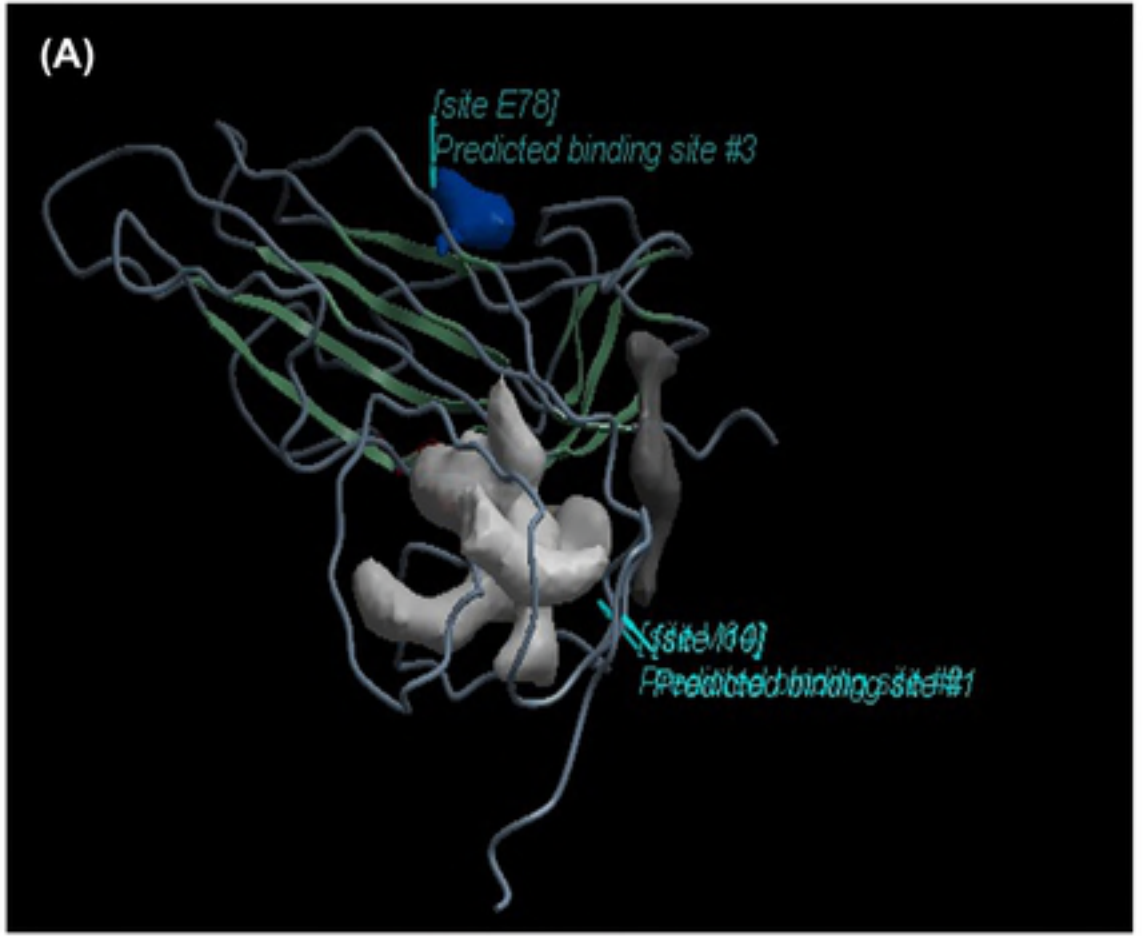

I14, V60, E78

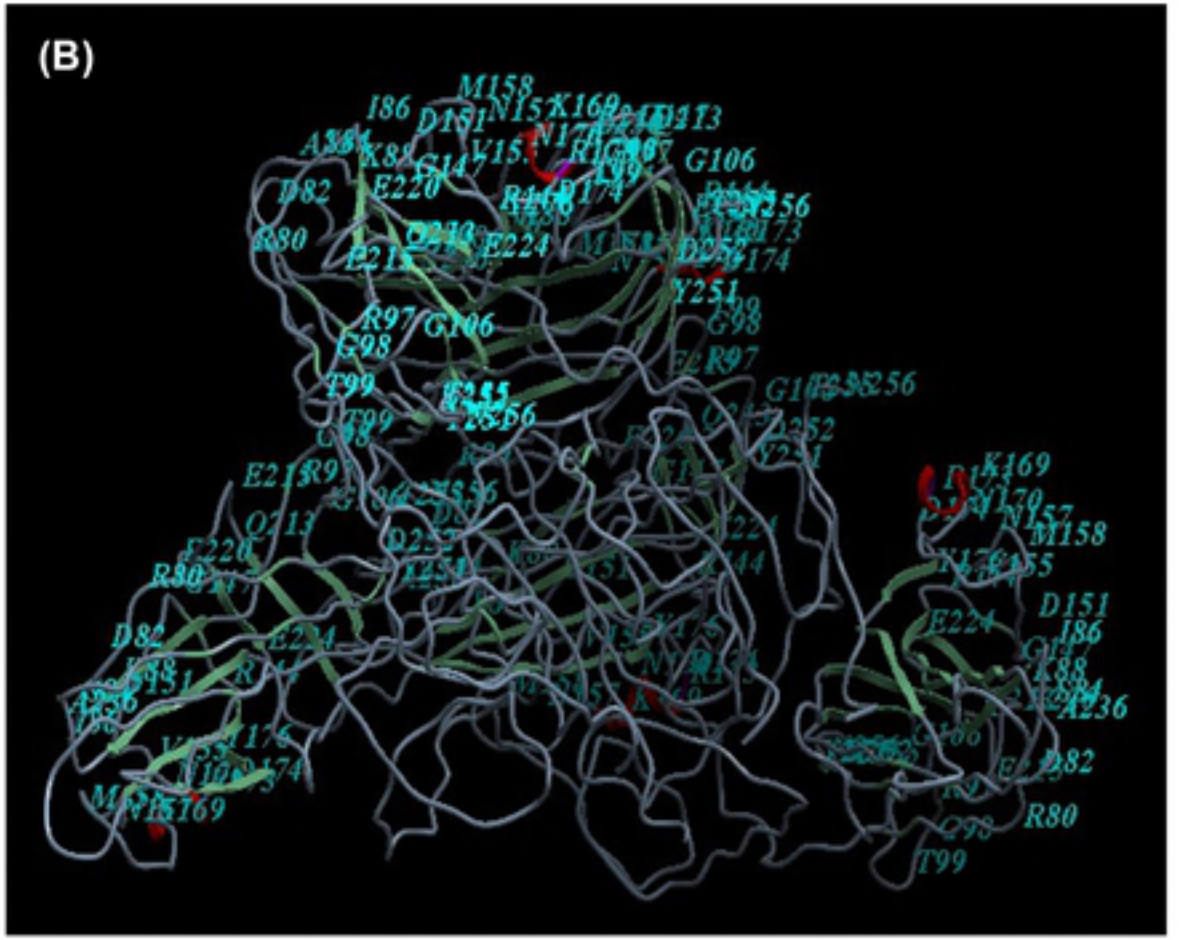

K169, Y176/Y251, D82/D151, E215/E220/E224, G98/G147, N157/N170, R97/R144 V155, T99

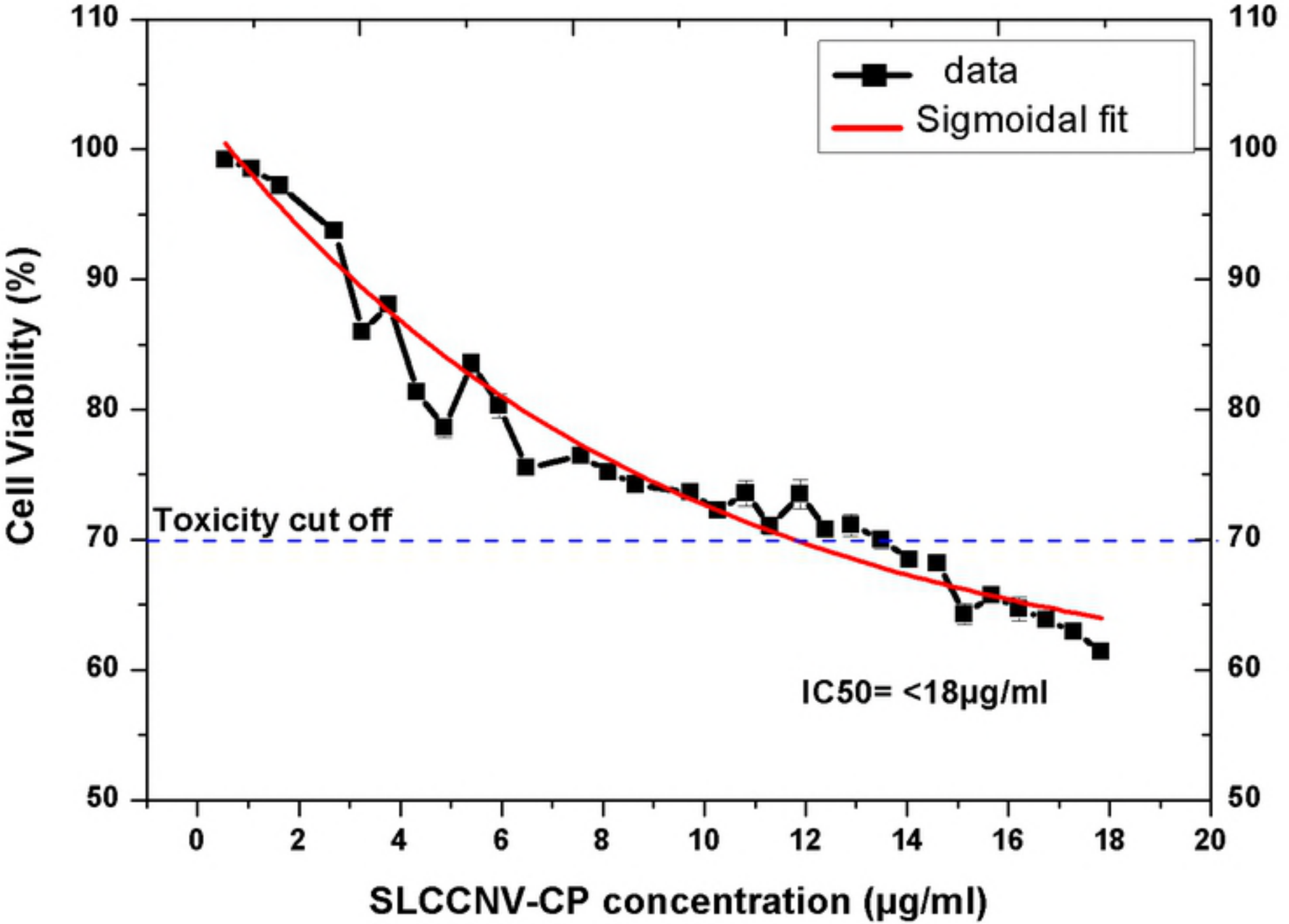
data
Sigmoidal fit
Toxicity cut off
IC50= <18µg/ml
Cell Viability (%)
SLCCNV-CP concentration (µg/ml)
110
100
90
80
70
60
50
0
2
4
6
8
10
12
14
16
18
20

bioRxiv preprint doi: https://doi.org/10.1101/338269; this version posted June 4, 2018. The copyright holder for this preprint (which was not certified by peer review) is the author/funder, who has granted bioRxiv a license to display the preprint in perpetuity. It is made available under aCC-BY 4.0 International license.

(A)

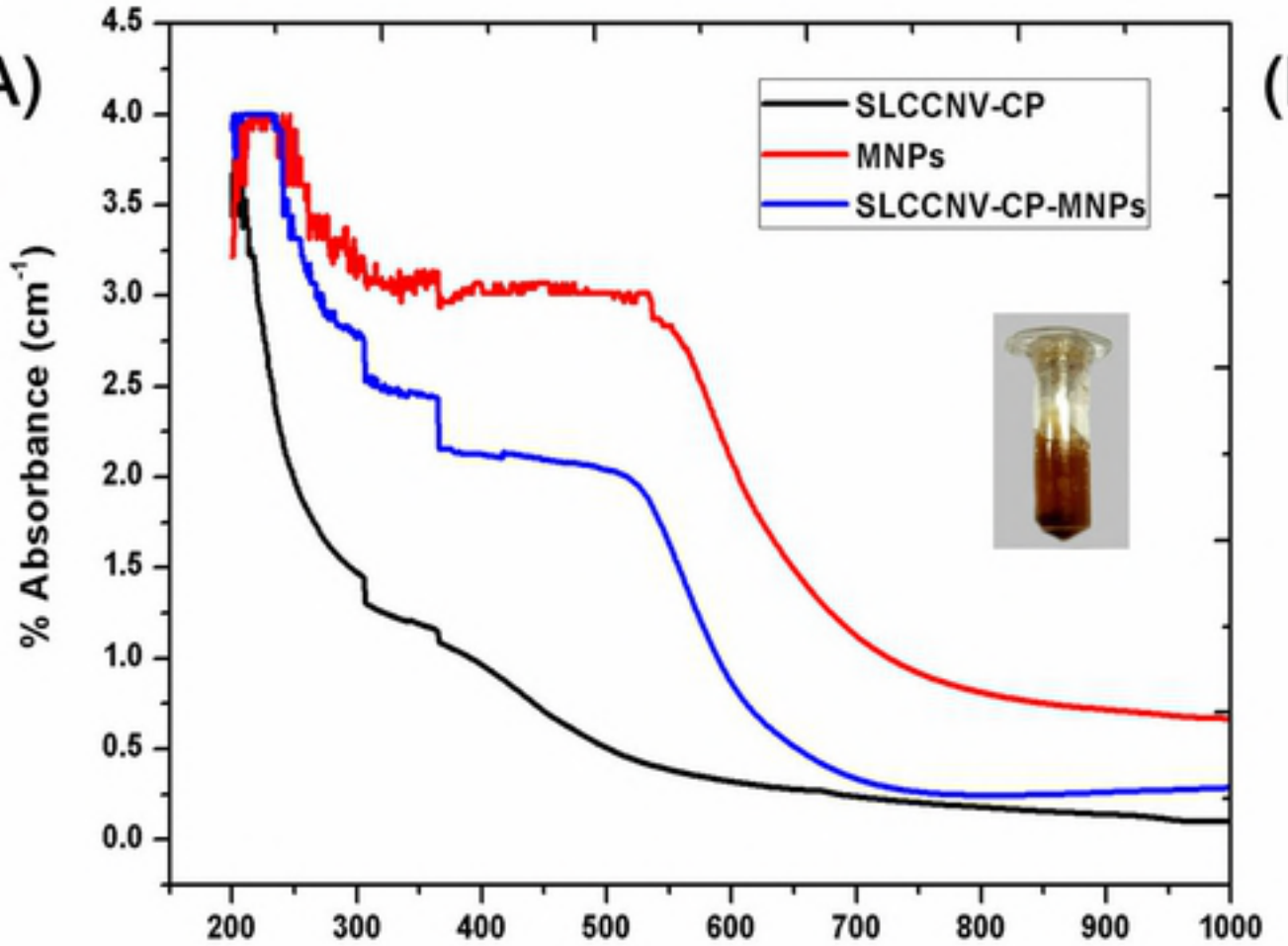

(B)

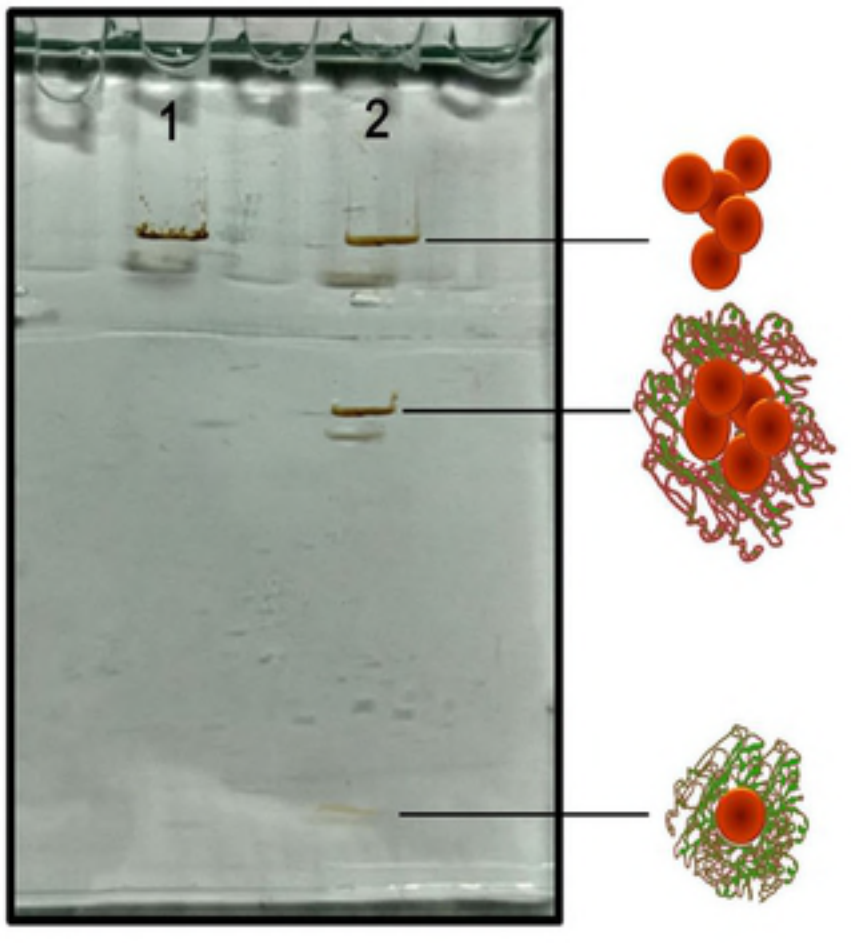

(C)

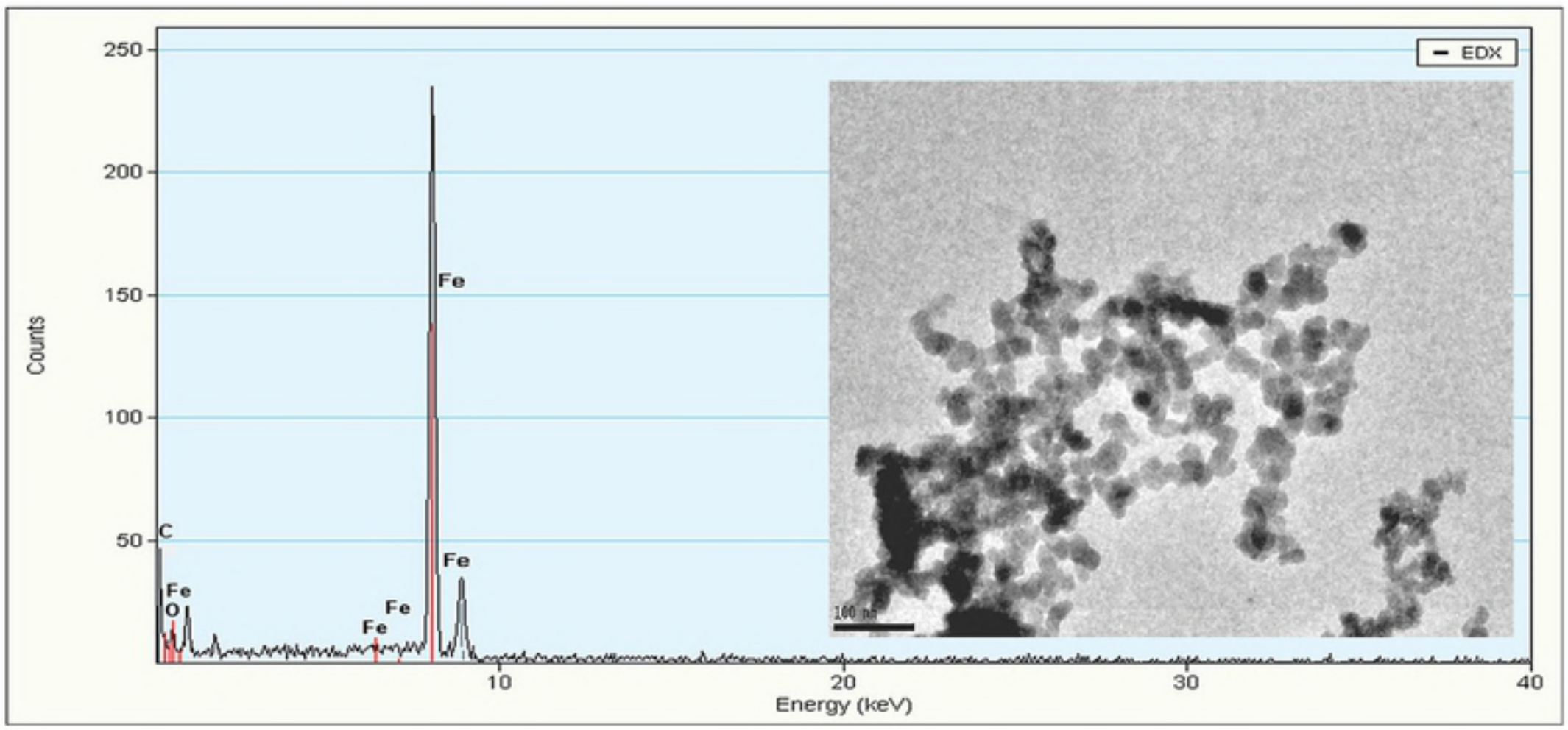

(D)

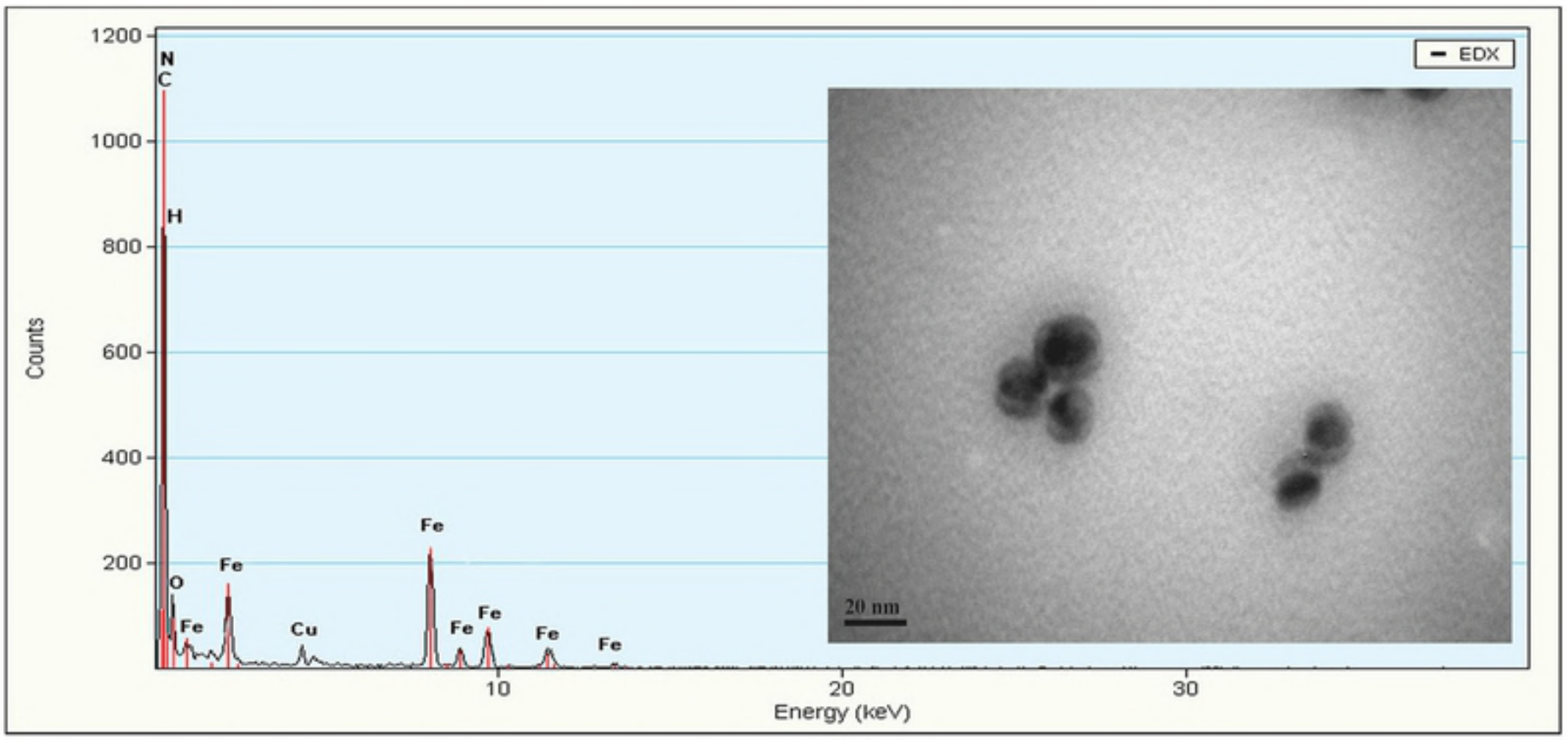

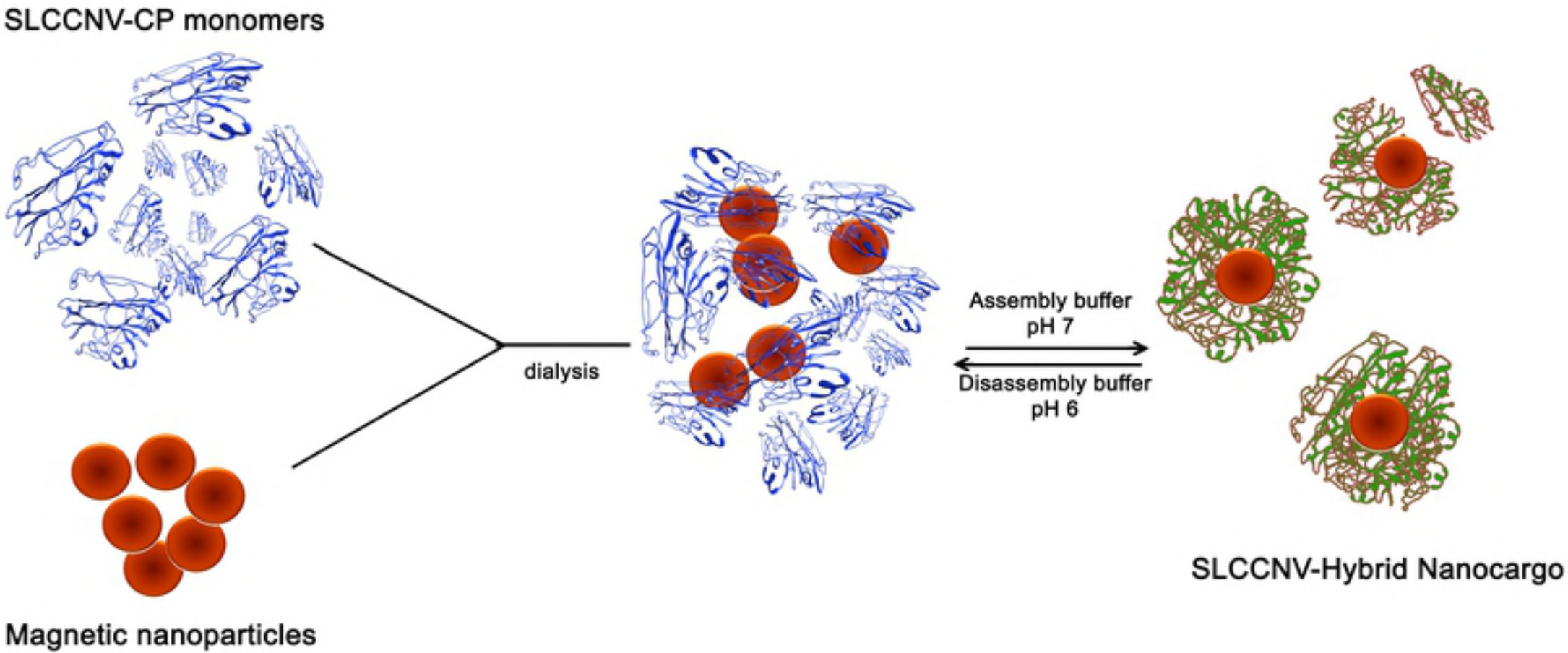
SLCCNV-CP monomers
Magnetic nanoparticles
dialysis
Assembly buffer
pH 7
Disassembly buffer
pH 6
SLCCNV-Hybrid Nanocargo

Nanocargo like virus structures
(Next generation Nanotool for Biomedical Application)

Begomovirus- Squash Leaf Curl China Virus

SLCCNV

Temperature
pH & Ionic strength
Denaturing Agent

Nano Cargo's conversion

viral genome

SLCCNV
Coat protein gene

pPICZ alpha A
vector

P. Pastoris Expression

Recombinant plasmid

SLCCNV- Expressed Coat protein

GTCAGA
CAGTCT

Bioinformatics

Structure & Assembly
prediction

"Nanocargo"
conversion

Magnetic nanoparticles
encapsulation

pH & Ionic strength dependent
assembly and disassembly

dialysis

Future prospects

Binding site prediction

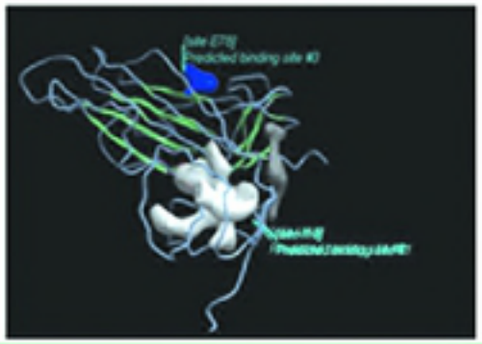

Bio-conjugation site prediction

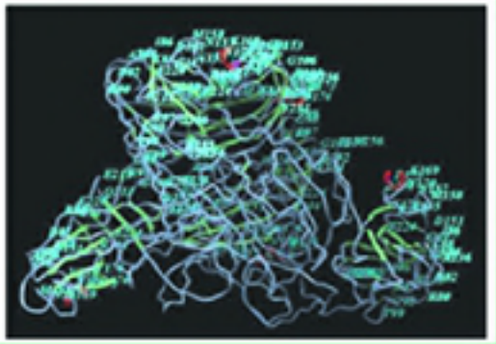

In vitro
Biocompatability assay